Cell Metabolism

Article

A cellular and molecular basis of leptin resistance

Graphical abstract

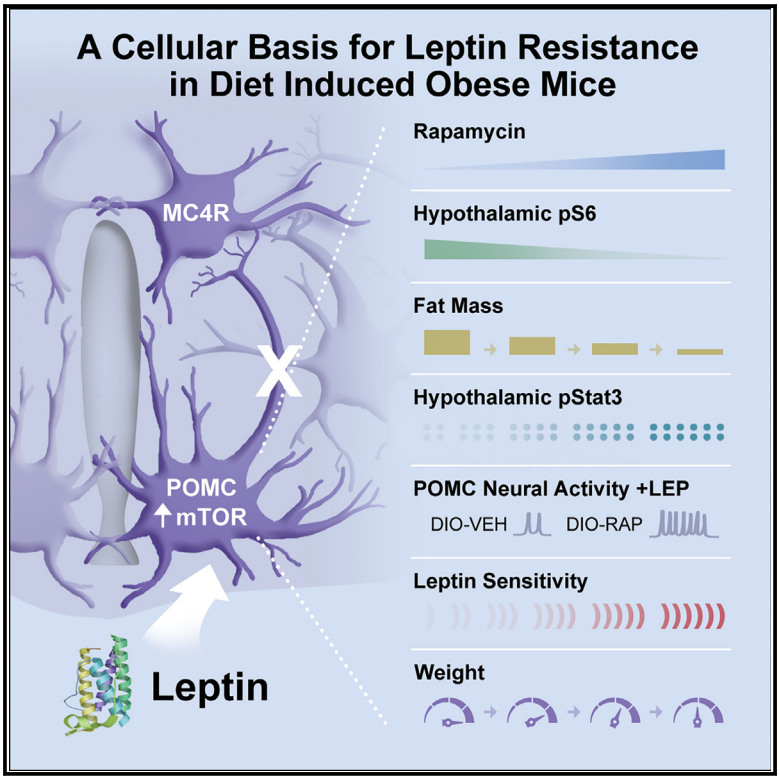

Highlights

- Rapamycin, an mTOR inhibitor, reduces food intake and fat mass in DIO mice
- Rapamycin's effect requires intact leptin-melanocortin signaling
- Rapamycin pre-treatment of DIO mice reverses leptin resistance in POMC neurons
- Increased mTOR activity in POMC neurons causes leptin resistance

Authors

Bowen Tan, Kristina Hedbacker, Leah Kelly, ..., Ji-Dung Luo, Joshua D. Rabinowitz, Jeffrey M. Friedman

Correspondence

friedj@rockefeller.edu

In brief

Tan and Hedbacker report that rapamycin, an mTOR inhibitor, reduces food intake and fat mass in diet-induced obese mice but not in leptin-deficient animals. Increased mTOR activity in POMC neurons caused leptin resistance, whereas rapamycin restored leptin's effects on POMC neurons, revealing a role for mTOR in leptin signaling.

Tan et al., 2025, Cell Metabolism *37*, 723–741
March 4, 2025
https://doi.org/10.1016/j.cmet.2025.01.001

CellPress

Cell Metabolism

CellPress
OPEN ACCESS

Article

A cellular and molecular basis of leptin resistance

Bowen Tan,[1,6] Kristina Hedbacker,[1,6] Leah Kelly,[1] Zhaoyue Zhang,[1] Alexandre Moura-Assis,[1] Ji-Dung Luo,[2] Joshua D. Rabinowitz,[3,4,5] and Jeffrey M. Friedman[1,7,*]

[1]Laboratory of Molecular Genetics, Howard Hughes Medical Institute, The Rockefeller University, New York, NY 10065, USA
[2]Bioinformatics Resource Center, The Rockefeller University, New York, NY 10065, USA
[3]Department of Chemistry, Princeton University, Princeton, NJ, USA
[4]Lewis-Sigler Institute of Integrative Genomics, Princeton University, Princeton, NJ, USA
[5]Ludwig Institute for Cancer Research, Princeton University, Princeton, NJ, USA
[6]These authors contributed equally
[7]Lead contact
*Correspondence: friedj@rockefeller.edu
https://doi.org/10.1016/j.cmet.2025.01.001

SUMMARY

Similar to most humans with obesity, diet-induced obese (DIO) mice have high leptin levels and fail to respond to the exogenous hormone, suggesting that their obesity is caused by leptin resistance, the pathogenesis of which is unknown. We found that leptin treatment reduced plasma levels of leucine and methionine, mTOR-activating ligands, leading us to hypothesize that chronic mTOR activation might reduce leptin signaling. Rapamycin, an mTOR inhibitor, reduced fat mass and increased leptin sensitivity in DIO mice but not in mice with defects in leptin signaling. Rapamycin restored leptin's actions on POMC neurons and failed to reduce the weight of mice with defects in melanocortin signaling. mTOR activation in POMC neurons caused leptin resistance, whereas POMC-specific mutations in mTOR activators decreased weight gain of DIO mice. Thus, increased mTOR activity in POMC neurons is necessary and sufficient for the development of leptin resistance in DIO mice, establishing a key pathogenic mechanism leading to obesity.

INTRODUCTION

Obesity is the cardinal feature of metabolic syndrome and a worldwide public health problem.[1] In lean animals, adipose tissue mass is tightly controlled by the hormone leptin (LEP), which functions as the afferent signal in a negative feedback loop that maintains energy balance. LEP reduces appetite, in part by activating α-MSH (POMC)-expressing neurons in the arcuate nucleus (ARC) of the hypothalamus. Most of the known mutations that cause obesity in humans and mice alter the production of α-MSH or its target, the MC4R G-protein-coupled receptor, leading to an inherited form of LEP resistance.[2,3] These LEP-resistant animals also show abrogated phosphorylation of the STAT3 transcription factor, a canonical biochemical marker of LEP signaling.[4–6]

LEP resistance also develops when mice are fed a high-fat diet (HFD) and become diet-induced obese (DIO), but the pathogenesis of this acquired form of LEP resistance is largely unknown. Similar to DIO mice, most humans with obesity also show resistance to LEP, and the response of DIO mice to anti-obesity therapies is highly predictive of a human response.[7,8] Thus, delineating a cause of LEP resistance in DIO mice would advance our understanding of the pathogenesis of obesity. Reversing LEP resistance could also have clinical implications, particularly because LEP spares lean body mass in contrast to the new peptide-based therapeutics that can cause significant loss of lean mass.[9] Here, we present a comprehensive set of physiologic, genetic, and neurobiological studies showing that increased activity of the mTOR kinase in POMC—and possibly other neurons—contributes to the development of LEP resistance and obesity in DIO mice.

RESULTS

A metabolomic screen for biomarkers for LEP resistance

Animals and humans with low LEP levels lose weight on LEP therapy, and we sought to identify acute biomarkers that predicted a LEP response as a possible means for identifying responders before weight loss develops (Figures 1A–1I and S1A–S1D).[3,7,8] We collected plasma from LEP-sensitive and LEP-resistant animals before and after LEP treatment: wild-type (WT) mice fed a chow diet (WT-chow) or a HFD (WT-DIO) and *ob/ob* mice fed a chow diet (OB-chow) or a HFD (OB-HFD). We controlled for food intake by pair-feeding the OB-chow group to chow-fed mice (WT-chow group) and by pair-feeding the OB-HFD group to DIO mice (WT-DIO group), all for 18 weeks (Figure 1A). Growth curves revealed that the WT-chow group remained lean whereas the other three groups became increasingly obese (Figures 1B, 1C, S1E, and S1F). Plasma was

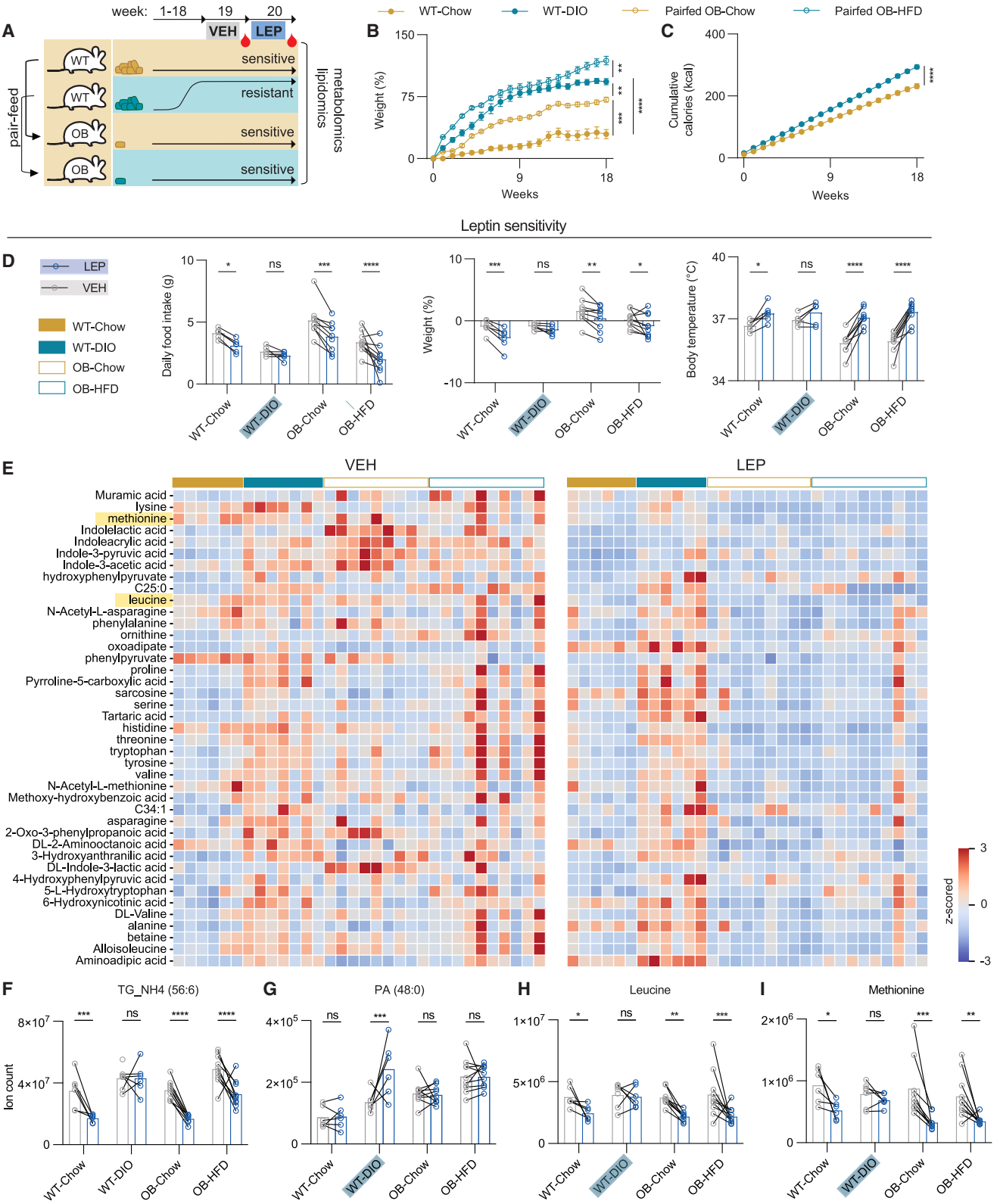

Figure 1. Metabolomic and lipidomic profiling of plasma metabolites associated with LEP resistance

(A) Schematic of *ob/ob* (OB) animals pair-fed to WT animals for 18 weeks fed a chow or HFD. At the 19th week, mice were i.p. injected with vehicle (VEH) every 12 h for 24 h, followed by blood collection. At the 20th week, mice were i.p. injected with 12.5 mg/kg leptin (LEP) every 12 h for 24 h, followed by blood collection. (B) Time-course percentage of body weight relative to starting point (week 0).

(legend continued on next page)

collected after vehicle (VEH) treatment at week 18 and again after LEP treatment at week 19 (Figure 1A). As expected, acute LEP treatment decreased food intake and body weight in the WT-chow, OB-chow, and OB-HFD groups, but not in LEP-resistant WT-DIO mice (Figure 1D). Plasma metabolites were measured and analyzed by first normalizing the samples at each time point, followed by hierarchical clustering based on levels of metabolites after LEP treatment (see heatmaps, Figures 1E, S1A, and S1B). These clustered heatmaps revealed a specific cluster of metabolites, including triglycerides and amino acids that were higher in the DIO group after LEP treatment vs. the other groups (Figures 1E, S1A, and S1B). As previously reported,[10] LEP decreased plasma triglycerides in LEP-sensitive mice but not in WT-DIO mice (Figures 1F and S1B). We also found increased levels of phosphatidic acids (PAs) and glucosyl ceramides after LEP treatment of WT-DIO mice, but these metabolites were unchanged in the other three groups (Figures 1G and S1B–S1D), raising the possibility that LEP prevented their accumulation in the sensitive animals. Finally, we found a significant decrease of plasma leucine and methionine levels in LEP-sensitive but not in LEP-resistant WT-DIO mice (Figures 1H, 1I, and S1A). Although the levels of other amino acids also changed, none showed significant differences between the DIO and other groups (Figures S2A–S2H). Leucine and methionine are canonical activators of mTOR signaling, and phosphatidic acids and ceramides can also modulate the phosphatidylinositol 3-kinase (PI3K)-mTOR pathway.[11–13] Our finding that LEP sensitivity was inversely associated with plasma levels of mTOR activators led us to hypothesize that mTOR activation might diminish LEP sensitivity in DIO mice. We evaluated this possibility by treating DIO mice with rapamycin (RAP), a specific mTOR inhibitor.

RAP reduces obesity by sensitizing DIO mice to LEP

DIO mice were treated with daily intraperitoneal (i.p.) injections of RAP or VEH for 10 weeks. The RAP-treated DIO mice showed a decrease in daily and cumulative food intake (RAP: 149.1 ± 4.1 g vs. VEH: 186.6 ± 5.5 g; $p < 0.001$), body weight (RAP: −27.6% ± 2.0% vs. VEH: 3.7% ± 2.1%; $p < 0.0001$), a marked decrease of fat mass (RAP: −11.1 ± 1.4 g vs. VEH: 4.2 ± 1.2 g; $p < 0.0001$), a small decrease in lean mass (RAP: −4.8 ± 0.4 vs. VEH: −1.0 ± 0.3; $p = 0.0514$), and a highly significant decrease in fat-to-lean ratio (RAP: −0.3 ± 0.1 a.u. vs. VEH: 0.2 ± 0.0 a.u.; $p < 0.0001$) (Figures 2A–2D and S3A). A similar decrease in lean mass after RAP has been previously reported, possibly due to inhibition of protein synthesis.[14,15] Thus, similar to the effects of LEP treatment of LEP-sensitive animals,[2] treatment of LEP-resistant DIO animals with RAP reduced food intake, body weight and preferentially reduced fat mass relative to lean mass (Figures 2C and 2D). We then tested whether pre-treating DIO mice with RAP restored their response to LEP.

We treated DIO mice with RAP for 3 weeks, followed by twice-daily injections of LEP or VEH for 3 days (Figure 2E). In DIO mice pre-treated with RAP, LEP injections elicited a further decrease in food intake compared with those pre-treated with VEH (Figure 2F, 9.6 ± 0.9 vs. 7.2 ± 0.9 g; $p < 0.01$), as well as decreased body weight (Figure 2G, 1.6% ± 0.5% vs. −2.9% ± 0.9%; $p < 0.01$) and a specific decrease in fat mass (Figures S3B and S3C). Because pre-treatment with RAP reduced the weight of DIO mice, and hence LEP levels (Figure 2H), a separate group of DIO mice were treated with VEH for 5 weeks while being pair-fed to the *ad libitum*-fed RAP-treated group on a HFD (Figure 2I). We then tested LEP sensitivity in these pair-fed animals. The response to LEP in the pair-fed DIO mice was significantly reduced compared with the RAP-treated group, with higher food intake (7.1 ± 0.6 vs. 5.1 ± 0.4 g; $p < 0.05$) and weight (+2.4% ± 1.3% vs. −2.1% ± 0.5%; $p < 0.01$). Consistent with their lower weight, the plasma LEP levels were lower in RAP-treated DIO mice compared with the pair-fed VEH group (19.1 ± 3.7 vs. 41.5 ± 3.2 ng/mL; $p < 0.01$) (Figures 2J–2L, S3D, and S3E). Indirect calorimetry revealed a decrease of respiratory exchange ratio (RER) in RAP-treated DIO mice (RAP 0.76 ± 0.00 RER vs. VEH 0.78 ± 0.01 RER; $p < 0.01$) and increased energy expenditure (RAP 1.2 ± 0.1 kcal/g vs. VEH 1.0 ± 0.0 kcal/g; $p < 0.05$) compared with the VEH group (Figures S3F–S3I).

As a further control, we fed DIO mice a HFD for 18 weeks, after which the diet was changed to chow, while simultaneously administering either RAP or VEH (Figure 2M). Consistent with prior reports,[16,17] when VEH-treated mice were switched from a HFD to chow, a significant reduction of body weight of ∼20% was observed (from 61.4 ± 1.0 to 48.1 ± 3.0 g; $p = 0.007$), associated with a decrease in fat mass and fat-to-lean ratio that plateaued by the 4th week at weights that were still considerably higher than chow-fed controls that had never been fed a HFD (35.0 ± 1.3 g; Figures 2N–2R; see Figure S1E). In contrast, DIO mice transferred to a chow diet while receiving RAP showed significantly greater weight loss, a greater reduction of fat mass, and a more sustained reduction in food intake than the VEH-treated group (from 58.2 ± 3.0 to 40.0 ± 2.2 g; $p < 0.0001$, Figures 2N–2R). These data suggest that RAP, but not weight loss (which develops after the mice are switched from a HFD to chow), can re-sensitize DIO mice to their endogenous LEP. If true, RAP should not affect food intake or fat mass in animals with defects in LEP signaling. We tested this by treating *ob/ob* (OB) and *db/db* (DB) mice with RAP.

Similar to 10 weeks of RAP treatment, DIO mice treated with RAP for 14 days showed a significantly decreased food intake

(C) Cumulative calories consumed (kcal) of WT mice fed a chow diet vs. a HFD over 18 weeks ($n = 6, 6$ for WT-chow, WT-DIO, respectively).
(D) Comparisons of 24-h food intake, 24-h % weight, and body temperature post VEH vs. post LEP ($n = 6, 6, 9, 10$ for WT-chow, WT-DIO, OB-chow, OB-HFD, respectively).
(E) Heatmap of the clustered metabolites' levels, higher in DIO post LEP vs. VEH. Comparisons of representative metabolites' levels (ion count) post VEH vs. post LEP.
(F–I) (F) TG_NH4 (56:6), (G) PA (48:0), (H) leucine, and (I) methionine (two-way ANOVA, with Fisher's LSD comparisons; $n = 6$ for WT-chow, $n = 7, 6$ for DIO that received VEH vs. LEP, $n = 9$ for OB-chow, $n = 10$ for OB-HFD).
(B and C) Two-way ANOVA with Tukey's multiple comparisons. (D and F–I) Two-way ANOVA with Fisher's LSD comparisons.
All error bars represent mean ± SEM. ns, not significant, $^{*}p < 0.05$, $^{**}p < 0.01$, $^{***}p < 0.001$, $^{****}p < 0.0001$.

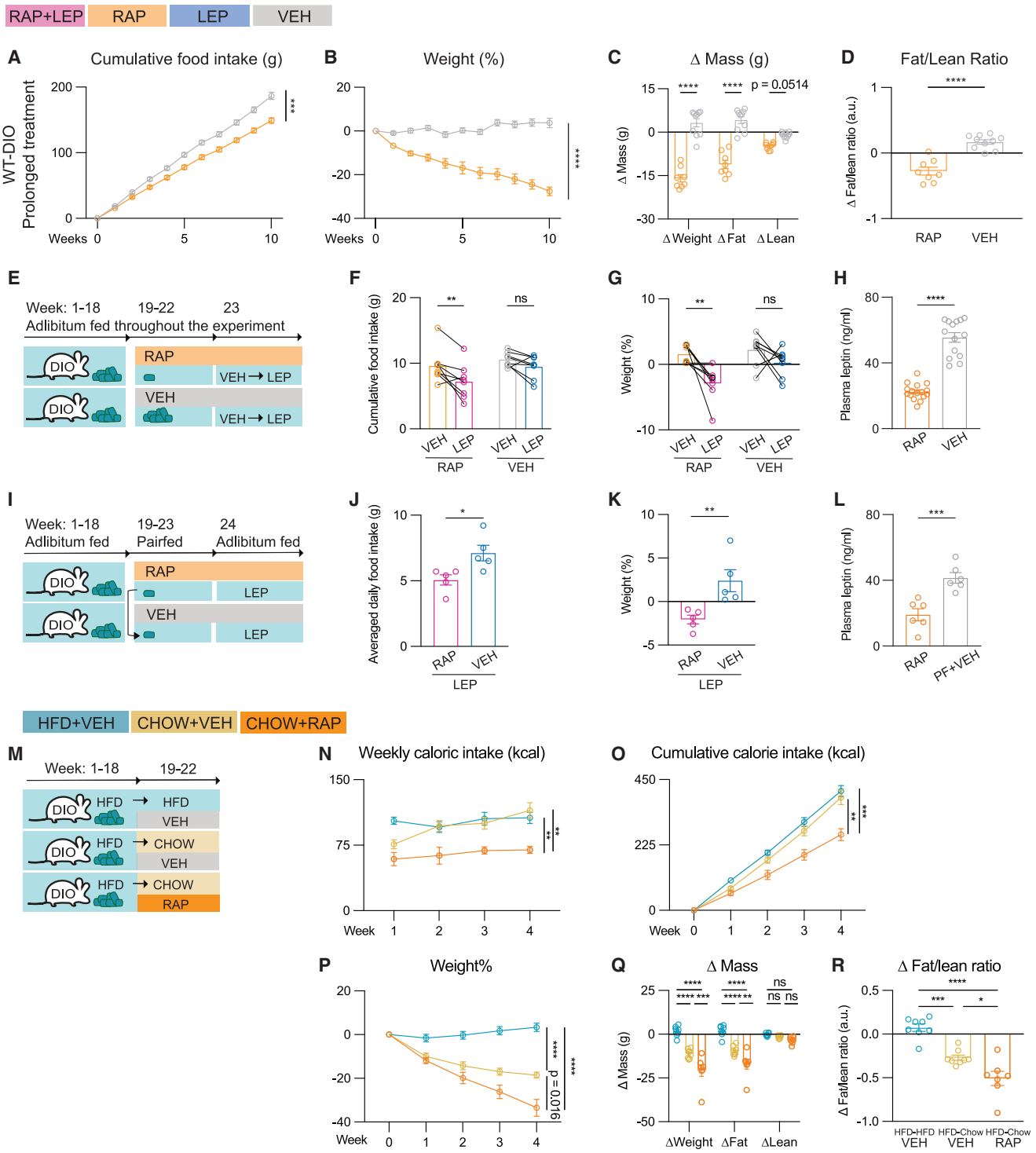

Figure 2. RAP reduces food intake, fat mass, and fat-to-lean ratio in DIO mice and increases their responses to the exogenous LEP

(A–D) WT-DIO prolonged treatment: DIO mice were treated daily with 2 mg/kg i.p. rapamycin (RAP) or vehicle (VEH) for 10 weeks. (A) Cumulative food intake and (B) weight; (C) Δ mass of weight, fat, and lean tissue; and (D) Δ fat/lean ratio (n = 9, 10, respectively, for cumulative food intake and weight; n = 8, 10 for Δ mass and Δ fat/lean ratio; two-way ANOVA, with Šidák's multiple comparisons for A–C; two-tailed Student's t tests for D; a.u. refers to arbitrary unit).

(E) Schematic of DIO mice that were treated with daily i.p. injections of 2 mg/kg RAP vs. VEH, followed by a leptin sensitivity test. Each group was treated with i.p. injections of VEH twice a day for 3 days, followed by 2 mg/kg LEP twice a day for 3 days.

(F and G) (F) Cumulative food intake and (G) weight during leptin sensitivity test (n = 8, 8 for each group; two-way ANOVA, with Šidák's multiple comparisons).

(legend continued on next page)

(RAP: 32.4 ± 1.6 g vs. VEH: 39.7 ± 1.9 g; $p < 0.001$), body weight (RAP: −10.2% ± 1.1% vs. VEH: 0.1% ± 1.1%; $p < 0.0001$), fat mass (RAP: −5.2 ± 1.3 vs. VEH: 0.5 ± 0.6; $p < 0.001$), and fat-to-lean ratio (RAP: −0.1 ± 0.1 a.u. vs. VEH: 0.1 ± 0.0 a.u, $p < 0.05$), with a small decrease in lean mass (Figures 3A–3D and S4A). In contrast, a 14-day course of RAP had little or no effect on food intake, body weight, or fat mass in lean, chow-fed mice that have low endogenous hormone levels (Figures 3E–3H and S4B). RAP also failed to decrease food intake or fat-to-lean ratio in *ob*/*ob* and *db*/*db* mice fed a chow or a HFD (Figures 3I–3P and S4C–S4J). RAP did lead to modest weight loss in *ob*/*ob* and *db*/*db* mice that was primarily limited to lean mass (in *ob*/*ob* Δweight: −3.9 ± 0.7 g, Δlean mass: −2.8 ± 0.2; *db*/*db* Δweight: −6.0 ± 2.1 g, Δlean mass: −5.6 ± 0.7 g), which was similar to the modest loss of lean mass observed in mice fed a HFD (Figures 3I–3P and S4C–S4P). We next tested whether LEP synergizes with RAP in lean or aged mice that also have lower LEP levels than DIO mice.

We compared the effects of high-dose (600 ng/h) to low-dose LEP (150 ng/h) in chow-fed mice, with or without RAP. As previously reported, the high dose of LEP resulted in a significantly greater decrease of weight and fat mass than did the lower dose (Figures S5A–S5D).[3] A combination of low-dose LEP (150 ng/h) with RAP elicited a significantly greater reduction of food intake, body weight, and fat mass than did low-dose LEP alone, and the final weight of the lean, chow-fed mice treated with low-dose LEP (150 ng/mL) plus RAP was comparable to that of mice treated with high-dose LEP (600 ng/h) (low-dose LEP + RAP vs. high-dose LEP; weight: −10.1% ± 1.0% vs. −8.6% ± 2.4%; p = ns, food intake: 59.8 ± 5.9 vs. 53.9 ± 3.4 g; p = ns, Δfat mass: −1.2 ± 0.3 vs. −1.0 ± 0.2 g; p = ns) (Figures S5E–S5H), with both groups showing a similar decrease in fat mass relative to lean mass (Figures S5C and S5G). These data show synergy between LEP and RAP in chow-fed mice.

Aged mice also develop obesity with modestly increased LEP levels.[18] Although chow-fed, aged mice weighed more than younger mice, 16-month-old animals were significantly less obese than DIO mice (aged weight: 39.8 ± 0.9 g, $n = 23$; DIO weight: 53.9 ± 0.9 g, $n = 19$, $p < 0.0001$; aged fat: 24.4% ± 1.5%, $n = 14$ vs. DIO fat: 45.1% ± 0.6%; $p < 0.0001$) with lower LEP levels (aged: 3.9 ± 1.0 vs. young: 1.3 ± 0.3 ng/mL LEP, see Figure S5I). We next compared the effect of high-dose LEP (600 ng/h), with or without RAP, in aged animals (Figures S5J–S5M). LEP alone resulted in a small but significant decrease of food intake, body weight, fat mass, and fat-to-lean ratio (Figures S5J–S5M). However, the addition of RAP to LEP significantly reduced food intake (LEP + RAP: 46.9 ± 3.8 g vs. LEP: 57.3 ± 4.8 g; $p < 0.05$), body weight (LEP + RAP: −13.8% ± 3.3% vs. LEP: −5.4% ± 2.8%; $p < 0.01$), and fat mass (LEP + RAP: −4.9 ± 0.5 g vs. LEP: −2.8 ± 0.5 g; $p < 0.05$), with no effect on lean mass ($p = 0.32$) (Figures S5J–S5M). RAP treatment of aged mice had no effect on food intake, body weight, or fat mass compared with VEH-treated mice (Figures S5N–S5Q).

Finally, we compared the effect of RAP with and without high-dose LEP in DIO mice. Consistent with their high baseline LEP levels (~48 ng/mL, Figure S6A), the food intake, body weight, and fat mass of DIO mice was similar in animals treated with RAP plus LEP (600 ng/h) vs. RAP alone (Figures S6B–S6E). However, the addition of LEP to RAP significantly improved glucose tolerance. RAP has been shown to impair glucose tolerance, whereas LEP has been shown to improve it.[19,20] Consistent with previous studies, chronic RAP treatment increased plasma glucose levels in chow-fed lean mice, *ob*/*ob* mice, and *db*/*db* mice, whereas a combination of LEP and RAP treatment lowered the baseline plasma glucose levels in WT-chow, WT-DIO, and OB-chow animals (Figures S6F–S6I). In these animals, RAP worsened glucose tolerance and the addition of exogenous LEP mitigated this (Figures S6J–S6M), with a lower peak glucose level in the chow-fed mice, a reduction of the area under the curve in DIO and chow-fed mice (WT-chow: RAP $5.4 \times 10^4 \pm 0.3 \times 10^4$ a.u. vs. RAP + LEP $3.2 \times 10^4 \pm 0.2 \times 10^4$ a.u.; $p < 0.0001$; DIO: RAP $9.3 \times 10^4 \pm 0.9 \times 10^4$ a.u. vs. RAP + LEP $6.9 \times 10^4 \pm 0.5 \times 10^4$ a.u.; $p < 0.05$), and the normalization of plasma glucose after 90–120 min in both DIO and chow-fed mice (Figures S6J–S6M).

In aggregate, these data show that RAP synergizes with exogenous LEP in chow-fed and aged mice that have lower baseline hormone levels. In addition, LEP treatment improved the glucose intolerance associated with RAP treatment. We next set out to establish the mechanism responsible for the re-sensitization of LEP signaling in DIO mice after RAP treatment.

The cellular target of RAP-mediated LEP sensitization

We mapped anatomic sites showing increased mTOR activity in DIO mice using whole-brain imaging for phosphoS6 (pS6),[21] a canonical marker for mTOR activity. The hypothalamus showed a significant increase of pS6 levels in DIO mice compared with chow-fed mice (Figures S7A and S7B). Because

(H) Plasma leptin in DIO mice after 3-week RAP vs. VEH treatment prior to a leptin sensitivity test ($n = 16, 14$ for RAP, VEH, respectively; two-tailed Student's t tests).

(I) Schematic of DIO mice that were treated with daily i.p. injections of RAP vs. VEH. The group of mice treated with VEH were pair-fed to the group of mice treated with RAP for 5 weeks. Leptin sensitivity test was conducted after 5-week treatment. For the leptin sensitivity test, each group of mice were treated with i.p. injections of 2 mg/kg LEP twice daily for 3 days followed by i.p. injections of VEH twice daily for 3 days. Both groups of mice had *ad libitum* access to food during the test).

(J and K) (J) Cumulative food intake and (K) weight of RAP vs. pair-fed VEH-treated DIO mice following i.p. injections of leptin ($n = 5, 5$; two-tailed Mann-Whitney tests).

(L) Plasma leptin in DIO mice after 3-week RAP vs. pair-fed VEH treatment prior to the leptin sensitivity test ($n = 6, 6$ for each group; two-tailed Student's t tests).

(M) Schematic of DIO mice that either remained on HFD with daily i.p. VEH injections or were transferred to a chow diet and administered daily i.p. injections of RAP vs. VEH.

(N–R) (N) Weekly caloric food intake; (O) cumulative calorie intake; (P) weight; (Q) Δ mass of weight, fat, and lean tissue; and (R) Δ fat/lean ratio ($n = 8, 8, 7$ for HFD-HFD + VEH, HFD-chow + VEH, HFD-chow + RAP, respectively; two-way ANOVA, with Tukey's multiple comparisons for N–Q; one-way ANOVA, with Tukey's multiple comparisons for R).

All error bars represent mean ± SEM. ns, not significant, $^*p < 0.05$, $^{**}p < 0.01$, $^{***}p < 0.001$, $^{****}p < 0.0001$.

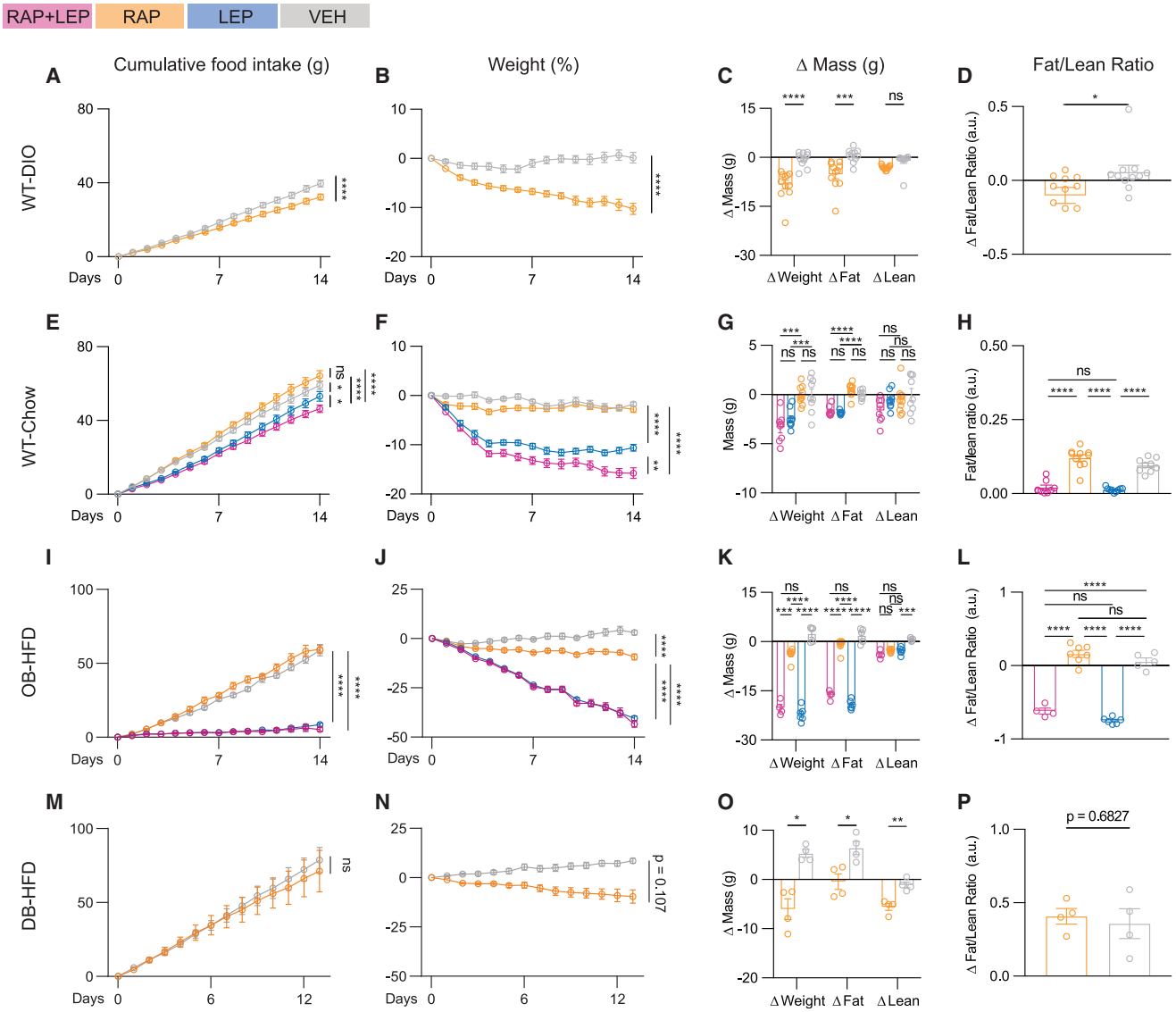

Figure 3. RAP reduces food intake, fat mass, and fat-to-lean ratio in DIO mice but not in *ob/ob* or *db/db* mice

(A–D) WT-DIO: DIO mice were treated with RAP or VEH daily for 14 days. (A) Cumulative food intake and (B) weight; (C) Δ mass of weight, fat, and lean tissue; and (D) Δ fat/lean ratio. (n = 9, 10 for RAP, VEH group, respectively, in A and B; n = 11, 11 for each group in C and D; two-way ANOVA, with Šidák's multiple comparisons for A–C; two-tailed Student's t tests for D.) WT-chow: chow-fed lean mice were treated with daily RAP plus 600 ng/h LEP, RAP plus VEH, LEP plus VEH, and VEH plus VEH for 14 days.

(E–H) (E) Cumulative food intake and (F) weight; (G) Δ mass of weight, fat, and lean tissue; and (H) fat/lean ratio at day 14. (n = 12, 14, 14, 13 for RAP + LEP, RAP, LEP, VEH, respectively, in E and F; n = 8, 10, 9, 9 for RAP + LEP, RAP, LEP, VEH, respectively, in G and H; two-way ANOVA with Tukey's multiple comparisons for E–G; one-way ANOVA with Tukey's multiple comparisons for H.) OB-HFD: *ob/ob* mice fed a HFD were treated with 2 mg/kg daily RAP plus 300 ng/h LEP, RAP plus VEH, VEH plus LEP, and VEH plus VEH for 14 days.

(I–L) (I) Cumulative food intake; (J) weight; (K) Δ mass of weight, fat, and lean tissue; and (L) fat/lean ratio (a.u.) at day 14. (n = 10, 13, 11, 10 for RAP + LEP, RAP, LEP, VEH, respectively, in I and J; n = 4, 7, 6, 5 for RAP + LEP, RAP, LEP, VEH, respectively, in K and L; two-way ANOVA with Tukey's multiple comparisons for I–K; one-way ANOVA with Tukey's multiple comparisons for L.) DB-HFD: *db/db* mice fed a HFD were treated with daily i.p. injections of RAP (2 mg/kg) vs. VEH for 13 days.

(M–P) (M) Cumulative food intake and (N) weight; (O) Δ mass of weight, fat, and lean tissue; and (P) Δ fat/lean ratio (a.u.), measured at days 0 and 13. (n = 4, 4, respectively; two-way ANOVA, with Šidák's multiple comparisons for M–O; two-tailed Student's t tests for P) (I)–(P) included female animals.

All error bars represent mean ± SEM. ns, not significant, *p < 0.05, **p < 0.01, ***p < 0.001, ****p < 0.0001.

LEP acts directly on the ARC,[6,22,23] we then assayed pS6 levels in ARC of DIO mice before and after RAP treatment using immunohistochemistry (IHC). Consistent with the data from brain clearing, pS6 levels were significantly elevated in the ARC of DIO mice vs. lean mice (Figure 4A). We then assayed pS6 levels in four groups (WT-chow, WT-DIO, OB-chow, and OB-HFD) receiving acute injections of VEH or LEP. These data showed that acute, high-dose LEP treatment significantly elevated

CellPress
OPEN ACCESS

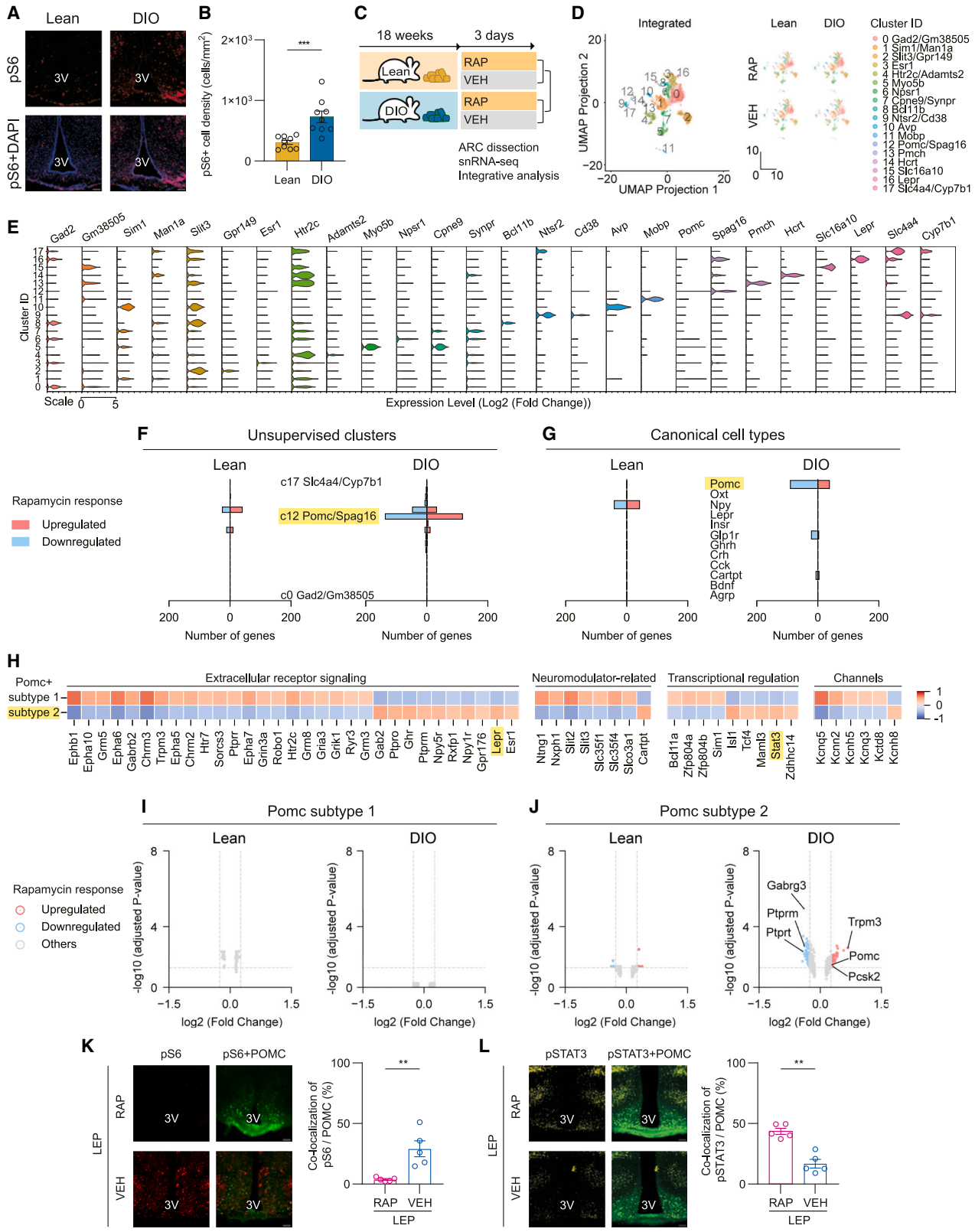

(legend on next page)

pS6 levels in the ARC of LEP-sensitive animals, including the WT-chow, OB-chow, and OB-HFD groups, but not in the LEP-resistant DIO group (Figures S7C and S7D).

We then performed single-nucleus RNA sequencing (snRNA-seq) of ARC after 3 days of RAP treatment vs. VEH in chow-fed lean, DIO, and chow-fed *ob*/*ob* mice (Figures 4C and S7E). This short-term treatment did not significantly alter food intake or body weight (Figures 3A, 3E, and S4A–S4D). Following microdissection of ARC, single-nuclei libraries were prepared and sequenced. Uniform manifold approximation and projection (UMAP) defined 18 distinct cellular clusters shared among all of the groups (Figure 4D) and generated a violin plot of enriched molecular markers for each (Figure 4E). These analyses revealed that RAP treatment of DIO mice significantly altered gene expressions only in cluster 12, which was defined by two marker genes, *Pomc* and *Spag16* (Figure 4F). The genes in this cluster showed only minimal changes in RAP-treated chow-fed mice and opposite effects were observed in *ob*/*ob* mice (Figures S7E–S7I). These data suggested that POMC neurons in this cluster might be a cellular target of RAP in DIO mice.

We further characterized the response to RAP by analyzing gene expression in ARC neurons expressing canonical marker genes, including *Pomc*+, *Oxt*+, *Npy*+, *Lepr*+, *Insr*+, *Glp1r*+, *Ghrh*+, *Crh*+, *Cck*+, *Cartpt*+, *Bdnf*+, and *Agrp*+ neurons (Figure 4G). Here, again, *Pomc*+ neurons from DIO mice showed the largest transcriptomic alterations in response to RAP (Figure 4G). Prior reports have indicated there are at least two distinct subsets of POMC neurons expressing either *Lepr* or *Glp1r*,[24–28] so we sub-clustered the POMC neurons into subtype 2 (corresponding to cluster 12), which included *Lepr*, *Stat3*, and *Spag16*, and subtype 1, which included *Htr2c* (Figure 4H). Only POMC subtype 2 showed significant transcriptional changes after RAP treatment of DIO mice (Figures 4H–4J), which decreased the expression of *Ptprm* and *Ptprt*, enzymes that dephosphorylate pSTAT3,[29] a key LEP signal transduction component, and *Gabrg3*, a GABA receptor subunit that inhibits POMC neurons.[30,31] RAP also increased the expression of *Pomc*, the α-MSH precursor; *Pcsk2*, a POMC processing enzyme; and *Trpm3*, a cation channel (Figure 4J). The expression levels of these genes were unchanged in POMC subtype 2 neurons from lean mice receiving RAP (Figure 4J), and *Pomc* and *Pcsk2* expression in these cells decreased in *ob*/*ob* mice (Figure S7H). This suggested that RAP restored LEP action by suppressing genes that diminish LEP signal transduction in POMC neurons and increasing those that increase the levels of α-MSH there. To assess this, we analyzed the levels of pSTAT3 and pS6 in POMC neurons after RAP in POMC-eGFP transgenic mice.[6] At baseline, pS6 levels were increased in POMC neurons of DIO mice and pSTAT3 was low (Figures 4K and 4L). After 3 days of RAP treatment, pS6 levels in POMC neurons decreased, whereas pSTAT3 levels significantly increased vs. controls (Figures 4K and 4L), suggesting that RAP re-sensitizes POMC neurons to endogenous LEP.

We next evaluated the response of POMC neurons to LEP in slices prepared from lean and DIO mice, DIO mice pre-treated with VEH for 3 days (DIO + VEH), and DIO mice pre-treated with RAP for 3 days (DIO + RAP). Representative cell-attached traces at baseline (Figure 5A) and before and after LEP application (100 nM, 20 min) to slices prepared from the four groups are shown. Firing rate was decreased in DIO mice vs. chow (0.92 ± 0.11 Hz, n = 155 vs. 2.00 ± 0.42 Hz, n = 51, p = 0.007) and DIO-VEH vs. chow (0.81 ± 0.20 Hz, n = 36 vs. 2.00 ± 0.42 Hz, n = 51, p = 0.003). RAP increased the firing rate in DIO-RAP relative to DIO-VEH (2.75 ± 0.64 Hz n = 28, vs. 0.81 ± 0.20 Hz, n = 36, p = 0.0004, all Mann-Whitney tests) (Figure 5B). DIO mice had a significantly smaller proportion of firing neurons compared with chow-fed mice (57.80%, n = 154 vs. 90.2%, n = 51, p < 0.0001, two-tailed binomial test) and RAP led to a significant increase in the number of spiking neurons compared with mice receiving VEH (90.2%, n = 51 vs. 47.22%, n = 36; p < 0.0001, both binomial tests) (Figure 5C). Overall, LEP led to a significant 49% increase in firing rate of POMC neurons from lean mice (2.95 ± 0.34 Hz n = 20 vs. 4.41 ± 1.31 Hz; n = 20; p = 0.028) (Figures 5D and 5E), with a smaller 18% increase in firing rates of neurons from DIO mice (1.50 ± 0.29 vs. 1.77 ± 0.33 Hz; n = 50 for both; p = 0.0238). Neurons in slices prepared after RAP pre-treatment showed a 38% increase in firing rate after LEP (3.58 ± 0.88 to 4.81 ± 1.03 Hz; n = 18, p = 0.0208) (Figure 5E), whereas the firing rate of DIO + VEH mice did not change significantly after application of LEP (1.38 ± 0.31 vs. 1.87 ± 0.67 Hz; n = 18; p = 0.6095) (Figure 5E). RAP treatment also significantly increased the proportion of LEP-excited neurons to 76.5%

Figure 4. snRNA-seq reveals that hypothalamic POMC neurons primarily respond to RAP in a LEP-signaling-dependent manner

(A) Immunohistochemical staining of pS6 (red) levels and DAPI (blue) in DIO mice compared with chow-fed lean mice. Scale bar: 100 μm.

(B) Quantification of pS6 densities in DIO mice compared with chow-fed lean mice (n = 9 sections from 3 mice for each group, two-tailed Mann-Whitney tests).

(C) Schematic of chow-fed lean mice or DIO mice followed by 3-day daily i.p. injections of 2 mg/kg RAP vs. VEH. 4-h after last treatment, ARC tissues were microdissected for snRNA-seq with integrated analysis across groups.

(D) UMAP representations of 18 clusters of cell types identified and shared across all lean-RAP, lean-VEH, DIO-RAP, and DIO-VEH groups (n = 4,934, 5,182, 5,992, 4,514 nuclei profiled from the ARC for each group).

(E) Violin plot depicting the expression levels of enriched molecular markers for each cluster.

(F and G) Quantification of total numbers of regulated genes by RAP vs. VEH across unsupervised clusters and canonical cell types.

(H) A heatmap representing the enriched molecular markers for POMC subtypes that are shared across all groups.

(I and J) Volcano plots showing differentially expressed genes in POMC subtypes in response to RAP vs. VEH between lean (I) and DIO (J) groups.

(K) Immunostaining of pS6 (red) and POMC-GFP (green) levels in DIOs that received 3-day RAP vs. VEH treatment, followed by acute leptin treatment (2 mg/kg, i.p. injections). Quantification of co-localization of pS6 and POMC-GFP (n = 5 sections from 3 mice for each group, two-tailed Mann-Whitney tests). Scale bar: 100 μm.

(L) Immunostaining of pSTAT3 (yellow) and POMC-GFP (green) levels in DIOs that received 3-day RAP vs. VEH treatment, followed by acute leptin treatment (2 mg/kg, i.p. injections). Scale bar: 100 μm. Quantification of colocalization of pSTAT3 and POMC-GFP (n = 5 sections from 3 mice for each group, two-tailed Mann-Whitney tests).

All error bars represent mean ± SEM. ns, not significant, *p < 0.05, **p < 0.01, ***p < 0.001, ****p < 0.0001.

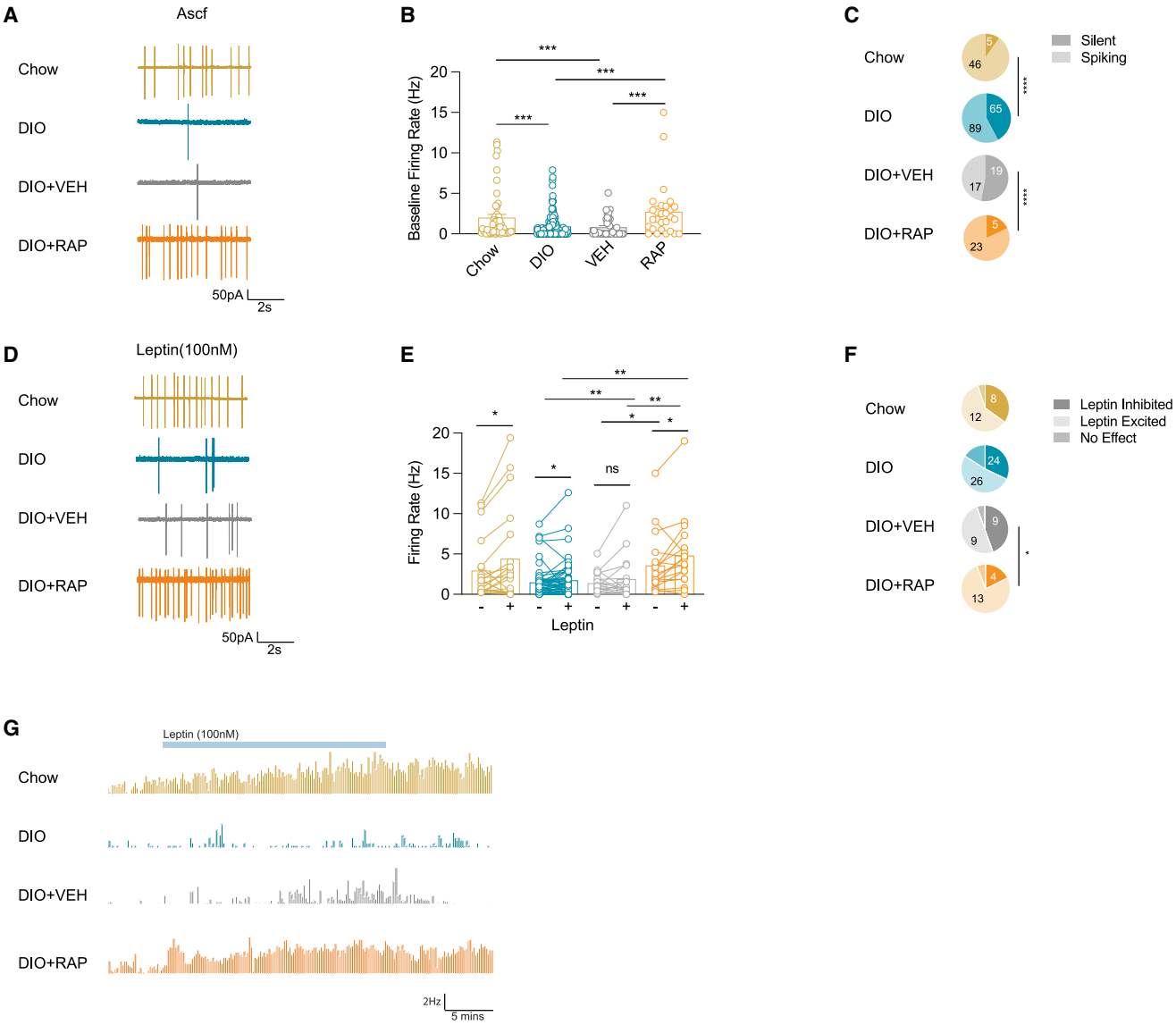

Figure 5. RAP increases baseline firing rate and proportion of LEP-excited POMC neurons in DIO mice

(A) Representative cell-attached recordings from a chow-fed, DIO, DIO treated with vehicle (DIO-VEH), and DIO treated with rapamycin (DIO-RAP) mouse (top to bottom). Scale bar represents 50 pA for chow and DIO, 100 pA for vehicle, and 20 pA for RAP, and 2 s for all traces.

(B) Baseline firing rate (Hz) of POMC neurons recorded from chow-fed, DIO, DIO-VEH, and DIO-RAP mice (left to right). Firing rate is decreased in DIO (n = 155; p = 0.007) and DIO-VEH (n = 36; p = 0.003) compared with chow-fed mice (n = 51). Rapamycin (n = 28) increased the firing rate compared with DIO (n = 155, $p < 0.0001$) and DIO-VEH (n = 36, p = 0.0004, all Mann-Whitney tests). Error bars represent mean ± SEM.

(C) Percentage of spiking POMC neurons is decreased in DIO (n = 154) and DIO-VEH (n = 36) compared with chow (n = 51; both $p < 0.0001$, two-tailed binomial test). Rapamycin increases the proportion of spiking POMC neurons compared with DIO mice (p = 0.012) and DIO-VEH ($p < 0.0001$, both binomial test).

(D) Representative cell-attached recordings from POMC-eGFP neurons after bath application of leptin (100 nM, 20 min) from chow-fed, DIO, DIO-VEH, and DIO-RAP mice (top to bottom). Scale bar represents 50 pA for chow and DIO, 100 pA for vehicle, and 20 pA for RAP, and 2 s for all traces.

(E) POMC firing rates (Hz) after bath application of leptin in aCSF (artificial cerebrospinal fluid, 100 nM, 20 min) recorded from chow-fed, DIO, DIO-VEH, and DIO-RAP (left to right). Leptin increased firing rate in POMC neurons in chow-fed mice (n = 20; p = 0.028), in DIO mice (n = 50; p = 0.0238), and in DIO-RAP mice (n = 18, p = 0.0208). Mean firing rate of POMC neurons of DIO-VEH mice does not change in the presence of leptin (n = 18; p = 0.6095, all Wilcoxon matched pairs). Mean firing rate in leptin is higher in POMC neurons of DIO-RAP mice (n = 18) compared with DIO-VEH (n = 18; p = 0.0047) and untreated DIO 1.77 ± 0.33 Hz (n = 50; p = 0.0002, both Mann-Whitney test).

(F) Proportion of leptin-excited POMC neurons in chow-fed mice (n = 20), DIO mice (n = 50), DIO-VEH (n = 18), and DIO-RAP mice (n = 17) (from top to bottom). Rapamycin increases the proportion of leptin-excited neurons in DIO (n = 17) compared with DIO-VEH (p = 0.0148, two-tailed binomial test).

(G) Firing rate histograms for individual cells during bath application of leptin (100 nM, 20 min) from POMC neurons of chow fed, DIO, DIO-VEH, and DIO-RAP from top to bottom. Firing rate (Hz) is calculated in 10 s bins. Leptin (100 nM) is bath-applied for 20 min (indicated in the blue box). Calibration bar for the DIO mice is 1 Hz, whereas for all other traces it is 2 Hz and 5 min. *$p < 0.05$,**$p < 0.01$,***$p < 0.001$,****$p < 0.0001$.

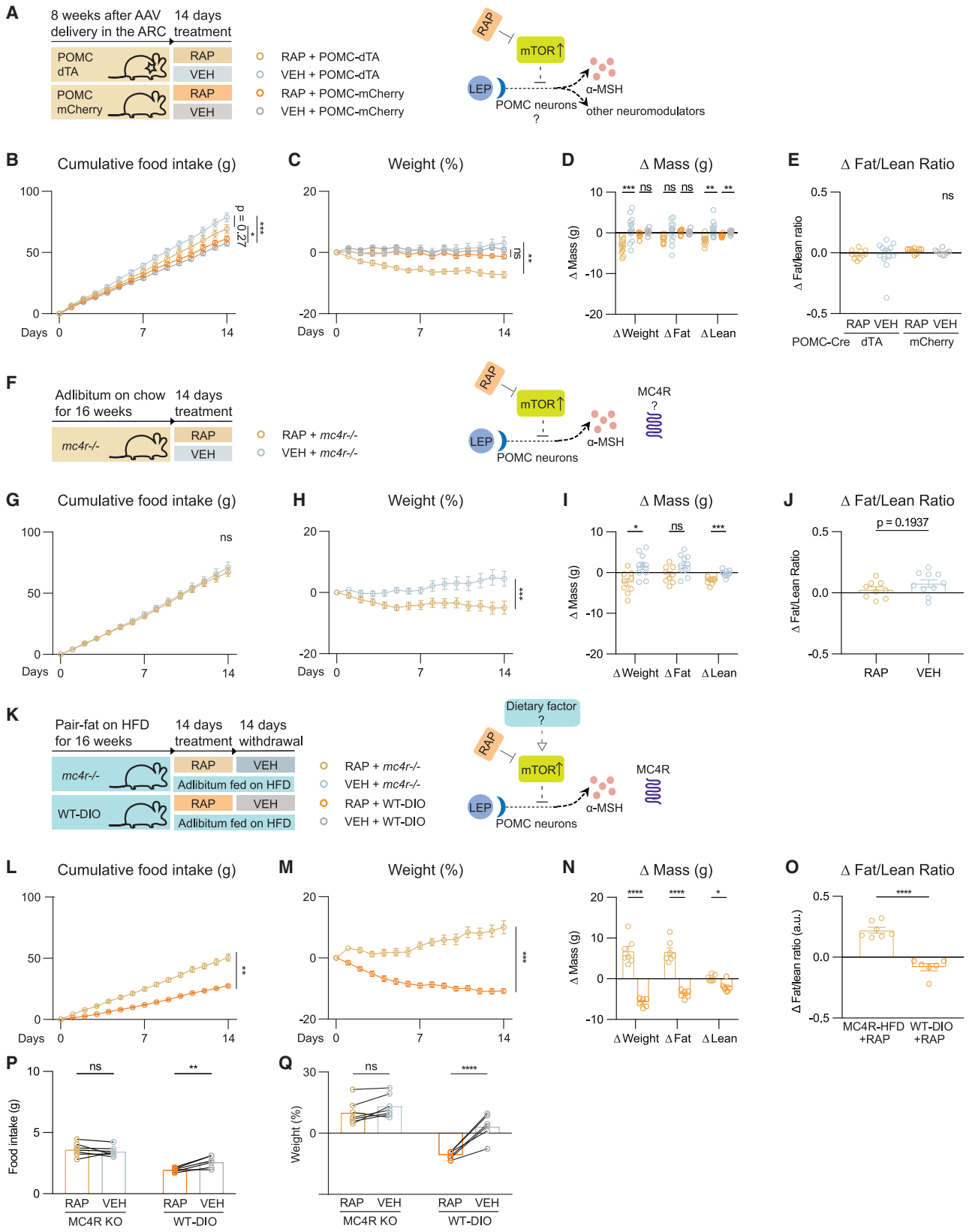

(legend on next page)

(n = 17; p = 0.0148, two-tailed binomial) compared with 50% in animals receiving VEH (n = 18; p = 0.0148, two-tailed binomial) (Figure 5F). In these experiments, mean firing rates before and after application of LEP were calculated in 10 s bins (see Figure 5G).

Melanocortin signaling is required for RAP-mediated LEP sensitization

Mice with an ablation of POMC neurons develop obesity,[32] and, if POMC neurons are a target of RAP, they should show a reduced response to RAP. We injected AAV5-hSyn-FLEX-mCherry or AAV5-hSyn-FLEX-dTA (diphtheria toxin A) into the ARC of POMC-Cre mice (referred to as POMC-dTA vs. POMC-mCherry mice, Figure 6A). 8 weeks post injection, POMC-dTA mice were obese (Figure S8A; POMC-dTA: 45.5 ± 2.0 g vs. POMC-mCherry: 29.0 ± 1.5 g), with a higher fat mass (42.5% ± 1.3% vs. 14.9% ± 2.3%; $p < 0.0001$), and POMC-mCherry mice remained lean. LEP treatment of POMC-dTA animals with a high dose of LEP (600 ng/h) had no effect on food intake or weight, confirming they are LEP resistant (Figures S8D–S8F). RAP treatment of POMC-dTA mice for 14 days did not significantly alter food intake (Figure 6B; RAP: 66.5 ± 4.2 g vs. VEH: 78.2 ± 3.3 g; p = 0.27), Δfat mass (−1.7 ± 0.3 vs. 0.2 ± 0.7 g; n = 11, 13, p = 0.12), or fat-to-lean ratio, though there was a small decrease in weight (RAP in dTA: −7.3% ± 1.1% vs. VEH in dTA: 3.1% ± 2.1%, $p < 0.01$) secondary to a reduced lean mass compared with VEH (RAP in dTA: −1.9 ± 0.3 g vs. VEH in dTA: 0.8 ± 0.5 g; $p < 0.01$; Figures 6C–6E and S8A). A combination of RAP and LEP also failed to alter food intake in the POMC-dTA animals (see Figures S8G–S8I).

Mice with a knockout of MC4R, the α-MSH receptor G-protein-coupled receptor (Figure 6F), develop obesity,[33] and, at baseline, *mc4r*−/− animals were hyperphagic, obese, and did not respond to LEP (Figures S8B and S8J–S8L). Similar to POMC-dTA mice, RAP did not reduce food intake in *mc4r*−/− mice (Figure 6G), and, although it induced a small decrease in body weight (−5.0% ± 2.1% vs. 4.5% ± 2.4%; $p < 0.001$), this was attributable to loss of lean mass (RAP: −2.0 ± 0.3 g vs. VEH: −0.2 ± 0.2; $p < 0.001$), with no significant effect on fat mass or fat-to-lean ratio (Figures 6H–6J and S8B). A combination of RAP and LEP also failed to reduce weight in *mc4r*−/− mutants vs. controls (Figures S8M–S8Q). Because *mc4r*−/− mice fed a HFD were more obese than DIO mice, we also controlled for possible weight effects by feeding *mc4r*−/− animals 10% fewer calories than were consumed by DIO animals (Figures 6K and S8C). These *mc4r*−/− animals are referred to as "pairfat" and, at 18 weeks, their weight was similar to DIO mice (Figure 6K). RAP-treated *mc4r*−/− pairfat mice consumed significantly more food than the RAP-treated DIO mice (*mc4r*−/−: 50.6 ± 2.9 g vs. DIO: 27.4 ± 0.9 g; $p < 0.01$) and even gained weight during the treatment (*mc4r*−/−: +10.1% ± 2.2% vs. DIO: −10.8% ± 0.7%; $p < 0.001$) (Figures 6L and 6M). After 14 days, fat mass and fat-to-lean ratios were significantly higher in RAP-treated *mc4r*−/− mice than in the RAP-treated DIO mice (Figure 6N; Δfat mass: *mc4r*−/−: 6.63 ± 1.9 g vs. DIO: −3.8 ± 0.4 g; $p < 0.0001$; fat-to-lean ratio: *mc4r*−/−: 0.2 ± 0.0 a.u. vs. DIO: −0.1 ± 0.0 a.u.; $p < 0.0001$), whereas lean mass did not change (Figures 6N and 6O). After cessation of RAP, the weight of DIO mice returned to pre-treatment levels, whereas that of the *mc4r*−/− mice did not change (Figures 6P and 6Q).

Increased mTOR activity in POMC neurons leads to LEP resistance

We next tested whether increased mTOR activity in POMC neurons is sufficient to cause LEP resistance by breeding POMC-Cre mice to *Tsc1-flox* mice. *Tsc1* encodes an endogenous mTOR inhibitor and germline *Tsc1* knockout mice show increased mTOR activity in numerous tissues (Figure 7A). Similar to previous reports,[34,35] chow-fed POMC$^{tsc1-/-}$ mice were hyperphagic and obese (Figures S9A–S9E), with increased endogenous LEP levels (POMC$^{tsc1-/-}$ 12.3 ± 3.4 ng/mL plasma LEP vs. 1.3 ± 0.4 ng/mL in controls; p = 0.0136, Figure S9F). In contrast to the response in control mice (POMC$^{tsc1+/-}$ and POMC$^{tsc1+/+}$), LEP did not reduce food intake or body weight in the POMC$^{tsc1-/-}$ mice (Figures 7B–7D), and pSTAT3 levels were significantly lower in the POMC$^{tsc1-/-}$ mice vs. controls following LEP treatment (Figure S9G). To control for possible effects of their obesity, we normalized the weight of the POMC$^{tsc1-/-}$ mice by pair-feeding them to the control mice. The pair-fed POMC$^{tsc1-/-}$ mice also failed to respond to LEP and even gained

Figure 6. RAP minimally regulates food intake, fat mass, and fat-to-lean ratio in obese mice models deficient in melanocortin signaling

(A) POMC ablation: schematic of POMC-dTA vs. POMC-mCherry mice that were treated with daily i.p. injections of 2 mg/kg (rapamycin) RAP vs. VEH for 14 days. Diagram of the interaction between the leptin, mTOR, and POMC neurons.

(B–E) (B) Cumulative food intake, (C) weight, (D) Δ mass of weight, fat, and lean tissue, and (E) Δ fat/lean ratio (a.u.) at days 0 vs. 14 (n = 10–11 for POMC-dTA + RAP, n = 11–13 for POMC-dTA + VEH, n = 8 for POMC-mCherry + RAP, n = 7–8 for POMC-mCherry + VEH; two-way ANOVA with Tukey's multiple comparisons tests for B–D; one-way ANOVA with Tukey's multiple comparisons for E).

(F) MC4R knockout: schematic of *mc4r*−/− mice fed a chow diet treated with daily i.p. injections of RAP (2 mg/kg) vs. VEH for 14 days. Diagram of the interaction between the leptin, mTOR, and POMC-MC4R pathway.

(G–J) (G) Cumulative food intake, (H) weight in chow-fed *mc4r*−/− mice; (I) Δ mass of weight, fat, and lean tissue; and (J) Δ fat/lean ratio (a.u.) at days 0 vs. 14 (n = 8, 10, for RAP, VEH groups, respectively, for G and H; n = 9, 10, for RAP, VEH groups, respectively, for I and J; two-way ANOVA, with Šidák's multiple comparisons for G–I; two-tailed Student's t tests for J).

(K) Schematic of the study design: *mc4r*−/− mice fed a HFD pairfat to WT-DIO mice for 16 weeks, after which they were treated with 14-day daily 2 mg/kg RAP i.p. injections followed by another 14-day daily i.p. VEH injections. Both groups of mice had *ad libitum* access to HFD throughout the pharmacological treatment. Schematic diagram of testing diet-dependent effects of RAP in HFD-mc4r−/− obese mice. Pairfat *mc4r*−/− and WT-DIO mice were treated with daily i.p. injections of RAP (2 mg/kg) for 14 days while *ad libitum*-fed on HFD.

(L–O) (L) Cumulative food intake and (M) weight; (N) Δ mass of weight, fat, and lean tissue; and (O) Δ fat/lean ratio (a.u.) at days 0 and 14.

(P and Q) (P) Averaged daily food intake and (Q) weight in (previously pairfat) *mc4r*−/− vs. WT-DIO mice after withdrawal from RAP followed by VEH for 14 days (n = 7 for pairfat *mc4r*−/− mice, n = 6 for WT-DIO mice; two-way ANOVA, with Šidák's multiple comparisons for L–N, P, and Q; two-tailed Student's t tests for O). (G)–(Q) included female animals.

All error bars represent mean ± SEM. ns, not significant, *$p < 0.05$, **$p < 0.01$, ***$p < 0.001$, ****$p < 0.0001$.

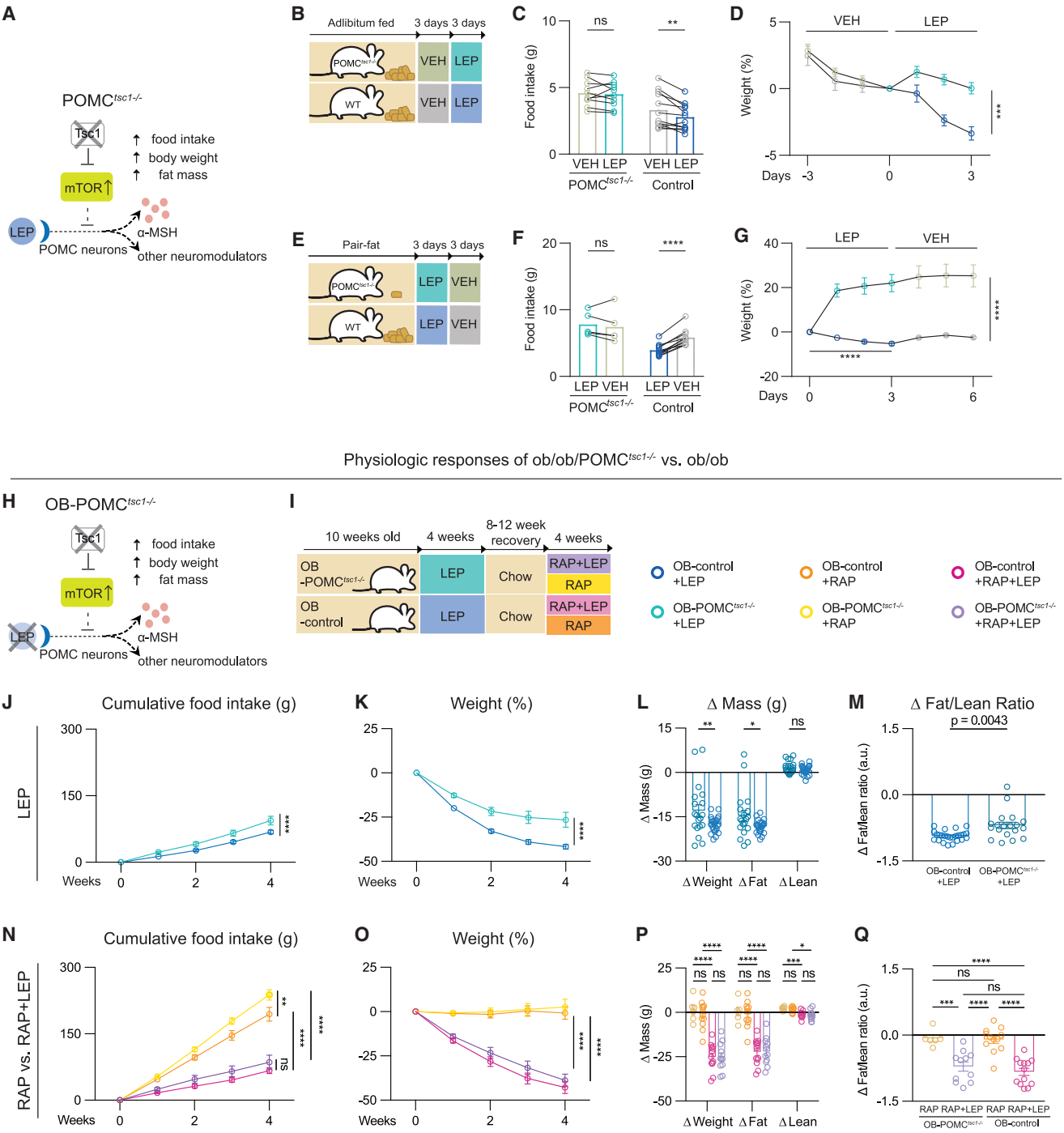

Figure 7. Genetic upregulation of mTOR activity in POMC cells causes LEP resistance, which is reversed by RAP in a LEP-signaling-dependent manner

(A) Diagram illustrates the deletion of the *Tsc1* gene, resulting in mTOR activation in POMC cells and subsequent development of obesity.

(B) Schematic depicting the leptin (LEP)-sensitivity test in POMC$^{tsc1-/-}$ and WT littermate mice fed a chow diet. Both mice were treated with twice-daily i.p. injections of VEH for 3 days, followed by twice-daily i.p. injections of 0.5 mg/kg LEP for another 3 days.

(C and D) (C) Averaged daily food intake and (D) weight during the 3-day LEP-sensitivity test in POMC$^{tsc1-/-}$ vs. WT mice *ad libitum*-fed on chow (n = 10 for POMC$^{tsc1-/-}$ mice, n = 12 for WT control mice; two-way ANOVA, with Šidák's multiple comparisons).

(E) Schematic depicting LEP-sensitivity test in pairfat POMC$^{tsc1-/-}$ and WT mice fed a chow diet. Both groups were treated with twice-daily i.p. injections of 0.5 mg/kg LEP for 3 days, followed by twice-daily i.p. injections of VEH for another 3 days. Both groups of mice had *ad libitum* access to food throughout VEH and LEP treatment.

(legend continued on next page)

weight during LEP treatment (POMC$^{tsc1-/-}$: 25.3% ± 5.0% vs. control: −2.5% ± 0.6%; $p < 0.0001$). At the end of LEP treatment, pair-fed POMC$^{tsc1-/-}$ and control mice were switched to VEH and, whereas the food intake increased in controls, the food intake of the POMC$^{tsc1-/-}$ mice did not change (Figures 7E–7G).

ob/ob mice are ultra-sensitive to LEP administration, and we next tested whether increased mTOR activity in POMC neurons can induce complete or partial LEP resistance in them (Figures 7H and 7I). *ob/ob* animals that carried a POMC-specific knockout of *Tsc1* were generated and, at baseline, the *ob/ob*-POMC$^{tsc1-/-}$ double-knockout (referred to hereafter as OB-POMC$^{tsc1-/-}$) mice showed a slight increase of lean mass and body weight compared with *ob/ob* controls (OB-control) (Figure S9H), lean mass: OB-POMC$^{tsc1-/-}$ 22.3 ± 0.3 g vs. OB-control 19.8 ± 0.3 g; $p < 0.05$), though the adiposity was similar between the two groups (fat mass %: OB-POMC$^{tsc1-/-}$ 52.3% ± 0.7% vs. OB-control 50.9% ± 0.7%; $p = 1.0$). We treated both groups with exogenous LEP for 4 weeks (Figure 7I), and OB-POMC$^{tsc1-/-}$ animals showed a diminished response to LEP, with 37.4% greater food consumption (Figure 7J; 94.0 ± 9.7 vs. 68.4 ± 4.0 g; $p < 0.0001$), diminished weight loss (Figure 7K; −26.5% ± 4.2% vs. −41.7% ± 1.3%; $p < 0.0001$), higher fat mass (Figure 7L; −14.6 ± 1.8 vs. −19.1 ± 1.3 g), and higher fat-to-lean ratio (Figure 7M) vs. controls. We then treated both groups with RAP ± exogenous LEP (Figure 7I). RAP alone had no effect on fat mass in the absence of LEP, whereas the combination of RAP and LEP normalized the LEP response of OB-POMC$^{tsc1-/-}$ mice, with comparable reductions in food intake (Figure 7N, RAP + LEP: OB-POMC$^{tsc1-/-}$, 85.5 ± 16.2 g vs. OB-control, 66.5 ± 6.4 g; p = ns), body weight (Figures 7O and S9I, RAP + LEP: OB-POMC$^{tsc1-/-}$, −38.8% ± 3.6% vs. OB-control, −42.8% ± 3.3%; p = ns), fat mass (Figure 7P, RAP + LEP: OB-POMC$^{tsc1-/-}$, −22.1 ± 2.4 g vs. OB-control, −22.4 ± 2.0 g; p = ns), and fat-to-lean ratio (Figure 7Q) as controls.

We next evaluated the effect of increasing mTOR activity in AgRP neurons. In contrast to the severe early-onset obesity of POMC$^{tsc1-/-}$ mice, AgRP$^{tsc1-/-}$ mice showed only a modest increase in body weight with no change in daily food intake relative to controls (Figures S9J–S9N). In addition, pS6 levels in AgRP neurons were similar in chow-fed vs. DIO mice, and pSTAT3 levels in AgRP neurons were similar to those of DIO mice after RAP treatment (Figures S9O and S9P).

Finally, we evaluated whether mutations that blunt mTOR activation in POMC neurons reduce weight gain in DIO mice. Leucine and methionine activate mTOR via the GATOR2 complex, whereas the RHEB GTPase directly activates the mTOR kinase and is inhibited by TSC1 (Figure S10A).[36–39] POMC-specific knockouts of *Rheb* and *Wdr24*, a key component of the GATOR2 complex, were generated by delivering guide RNAs for these two genes, as well as control guide RNAs, into the ARC of POMC-Cas9 mice generated by mating POMC-Cre mice to lox-stop-lox (LSL)-Cas9 mice. Although there was no difference when the groups were fed a chow diet for 3 weeks (Figure S10B), the POMC-specific knockouts of *Wdr24* or *Rheb* (Figures S10B–S10D) consumed less food and gained less weight on a HFD (Figures S10B–S10F). In addition, the levels of pSTAT3 in the ARC were significantly higher in POMC-specific knockouts of *Wdr24* or *Rheb* mice after LEP treatment vs. controls (Figures S10G and S10H). Thus, consistent with the effect of inhibiting mTOR with RAP, CRISPR-mediated knockouts of these mTOR activators in ARC^{POMC} neurons attenuated the development of diet-induced obesity.

DISCUSSION

DIO mice develop LEP resistance, the cause of which is unknown.[3,7,8] In an initial metabolomic screen for biomarkers indicative of a LEP response, we found that the levels of several mTOR-activating ligands inversely correlate with LEP sensitivity, leading us to test whether increased mTOR activity might contribute to LEP resistance. We found that RAP, a specific mTOR inhibitor, reduces body weight in DIO mice but not in mice with defects in LEP signaling or low circulating levels of the hormone. We then employed snRNA-seq to show that RAP treatment of DIO, but not lean mice, specifically induced gene expression in POMC neurons that promote LEP signaling and melanocortin production. Further studies showed that POMC neurons and melanocortin signaling are necessary for RAP's weight reducing effects and that increased mTOR activity in POMC neurons is sufficient to cause LEP resistance. These data establish a cellular and molecular basis for LEP resistance in DIO mice.

These conclusions are consistent with genetic studies of obesity showing that defects in LEP-melanocortin signaling cause obesity.[32,33,40] POMC encodes a protein precursor that is processed by proteases PCSK1/2 to generate α-MSH, which can potently reduce food intake and body weight through broadly distributed receptors in the brain, including MC4R.[41–44] Mutations in *Pomc*, *Pcsk1*, and *Mc4r* all cause severe early-onset obesity in humans,[33,40] resulting in an inherited form of

(F and G) (F) Averaged daily food intake and (G) weight during the 3-day LEP-sensitivity test in POMC$^{tsc1-/-}$ vs. WT mice *ad libitum*-fed on chow (n = 5 for POMC$^{tsc1-/-}$ mice, n = 11 for WT control mice; two-way ANOVA, with Šidák's multiple comparisons).
(H) Diagram illustrates a complete loss of LEP signaling in *ob/ob*/POMC$^{tsc1-/-}$ mice.
(I) Schematic of *ob/ob*/POMC$^{tsc1-/-}$ (OB-POMC$^{tsc1-/-}$) and *ob/ob* controls (OB-control: *ob/ob* POMC-Cre+ *tsc1fl/−* and *ob/ob* POMC-Cre− *tsc1fl/fl*) mice fed on chow that were treated with 150 ng/h LEP for 4 weeks, followed by an 8- to 12-week recovery period. After recovery, these mice were treated with 150 ng/h LEP plus 2 mg/kg RAP (i.p. injections 3 times a week) vs. VEH plus 2 mg/kg RAP (i.p. injections 3 times a week).
(J–M) (J) Cumulative food intake and (K) weight during 4-week LEP treatment; (L) Δ mass of weight, fat, and lean tissue; and (M) Δ fat/lean ratio (a.u.) at week 0 vs. at the end of week 4 (n = 19 for OB-POMC$^{tsc1-/-}$, n = 25–26 for OB-control; two-way ANOVA, with Šidák's multiple comparisons for J–M; two-tailed Student's t tests for M).
(N–Q) (N) Cumulative food intake and (O) weight during 4-week treatment; (P) Δ mass of weight, fat, and lean tissue; and (Q) Δ fat/lean ratio (a.u.) at week 0 vs. at the end of week 4 in OB-POMC$^{tsc1-/-}$ vs. OB-control (n = 11 for RAP + LEP in OB-POMC$^{tsc1-/-}$, n = 13 for RAP + LEP in OB-control, n = 6 for RAP + VEH in OB-POMC$^{tsc1-/-}$, n = 12–13 for RAP + VEH in OB-control; two-way ANOVA, with Šidák's multiple comparisons for N–P; two-tailed Student's t tests for Q). (J)–(Q) include female animals.
All error bars represent mean ± SEM. ns, not significant, *$p < 0.05$, **$p < 0.01$, ***$p < 0.001$, ****$p < 0.0001$.

LEP resistance. Our data indicate that defects in this same pathway can also be acquired when mice are fed a HFD. It is not yet clear why this diet leads to increased mTOR activity in POMC neurons, but a previous study has suggested that sustained hyperleptinemia can cause LEP resistance.[45–47] We hypothesize that weight gain after consumption of a palatable diet by C57BL/6J mice (and other strains that are obesity prone) leads to a sustained increase in LEP levels, in turn increasing mTOR activity as a means of blunting the response (i.e., tachyphylaxis), as has also been suggested for other hormones, including insulin.[48] However, further studies currently underway will be necessary to assess this, and it is also possible that other mechanisms contribute.

Consistent with a role for mTOR in causing LEP resistance, our studies, as well as prior studies of mice with a deletion of *Tsc1* in POMC neurons, revealed that increased mTOR activity in these neurons causes obesity that is ameliorated by RAP.[34,35] A previous study also showed that intracerebroventricular (ICV) infusion of RAP reduced food intake and body weight in aged mice,[34] although we found that daily i.p. injections of RAP alone did not reduce food intake or fat mass relative to lean mass, except when combined with exogenous LEP treatment. The difference between this prior study and ours may be due to the use of different RAP dosages and routes of administration. Furthermore, this previous study did not assess whether RAP reduced weight by restoring LEP signaling *in vivo* nor did it establish the importance of mTOR hyperactivity in POMC neurons as a cause of diet-induced obesity, the pathogenesis of which, as mentioned, is considered to be similar to human obesity. We also observed increased POMC neural activity and LEP responsiveness after RAP treatment using electrophysiology. However, because DIO mice need to be fed a HFD for several months, we cannot assess the extent to which aging might also contribute to the reduced POMC neural activity and LEP responsiveness that we observed in the slice preparations.

Our conclusions are also consistent with several reports showing that RAP and low leucine or methionine diets attenuate diet-induced obesity, whereas mTOR activation in POMC neurons causes obesity.[49–51] However, in these prior studies, an effect on LEP sensitivity was not evaluated and the role of POMC neurons in mediating this response was not shown. Our data thus unify and extend a large number of prior studies by showing that increased mTOR signaling in POMC neurons is both necessary and sufficient for the development of diet-induced obesity and provides a mechanism explaining how and why RAP and low-protein diets reduce obesity. We also found that downregulation of the leucine-sensing GATOR2 complex in POMC neurons blunts weight gain in POMC-*Wdr24* mice fed a HFD. Consistent with this, we found that LEP reduced plasma levels of leucine and methionine in LEP-sensitive animals. However, further studies will be required to understand how LEP reduces these amino acid levels and establish whether this lowering contributes to LEP's effects.

Although an earlier report suggested that RAP blunted the acute effects of LEP, this study only evaluated the effect of a single dose of LEP on food intake and did not specify which neuronal type was responsible for the effect.[52] It is thus possible that, although transient mTOR activation may mediate some of LEP's acute effects, chronic mTOR activation, possibly induced by chronically high hormone levels, leads to a downregulation of LEP signaling. Consistent with this, we found that pS6 levels were low at baseline in chow-fed mice and that acute LEP treatment increased pS6 levels in the Arc (see Figures S7C and S7D), whereas chronic hyperleptinemia in DIO mice is associated with constitutively high pS6 levels.

We also found that increased mTOR activity in POMC neurons of *ob/ob* (by breeding to POMC$^{tsc1-/-}$ mice) leads to partial LEP resistance. However, LEP's effect, although reduced, is still significant in these mice, suggesting that the hormone acts on other target populations, including AgRP neurons. AgRP neurons drives food consumption and are inhibited by LEP. Our finding that DIO is caused by defects primarily in POMC neurons is consistent with the fact that *ob/ob* mice are significantly more obese than DIO mice, likely as a result of LEP action at other cellular sites besides POMC neurons. However, in contrast to its effects in POMC neurons, increased mTOR in AgRP neurons only had a modest effect on weight and fat mass. Nonetheless, our data do not exclude the possibility that mTOR might also affect LEP signaling in these and additional cell types. We observed increased pS6 levels in a number of hypothalamic sites within and outside the ARC in DIO mice, such as the ventromedial hypothalamus and preoptic areas, as well as in the basomedial amygdala and striatum. It is not clear which of these neurons express the LEP receptor and what their possible contributions to LEP resistance are.

The data from single-nuclei sequencing suggest that chronic mTOR activation activates genes that diminish LEP signaling and that RAP reverses this. Consistent with this, we found that RAP increases the levels of pSTAT3 in POMC neurons, possibly by decreasing the expression of *Ptprm* and *Ptprt*, which dephosphorylate pSTAT3.[29] However, other mechanisms in addition to dephosphorylation of pSTAT3 may also contribute because a POMC-specific knockout of *Stat3* results in only a mild obese phenotype.[5,53] Other signaling molecules have been shown to contribute to LEP resistance, including SOCS3 and PIAS proteins that inhibit JAK and STAT activity, respectively, to decrease LEP signal transduction.[53–60] Another report suggested that increased mTOR signaling in POMC neurons increases the activity of an inhibitory K^{ATP} channel and that POMC neurons from POMC$^{tsc1-/-}$ mice are hyperpolarized via increased K^{ATP} conductance.[34] Other reports also show that increased levels of PIP3 can silence POMC neurons by increasing K^{ATP} channel activity.[61] Thus, increased expression of the K^{ATP} channel or similar channels could also reduce the activity of POMC subtype 2 neurons expressing the LEP receptor. *Grb10*, an endogenous mTOR inhibitor,[4,62] and HDAC6 have also been reported to modulate LEP sensitivity,[63] and impaired calcium influx, autophagy, increased reactive oxygen species, interleukin-1 (IL-1), and/or increased endoplasmic reticulum (ER) stress in POMC neurons have been reported to cause LEP resistance.[64–72] In addition, several GI hormones, including CCK, amylin, and dual and triple agonists, can also restore LEP action in DIO mice.[73,74] Further studies will be necessary to integrate these findings and establish whether these agents alter mTOR signaling in POMC and other neurons or whether additional mechanisms contribute.

RAP was first developed as an immunosuppressant,[75,76] but, more recently, it has been evaluated as a possible agent for

extending lifespan.[77] Increased BMI has been shown to be an independent risk factor for mortality,[78] raising the possibility that restored LEP sensitivity and reduced body weight could contribute to RAP's effect on longevity. However, RAP also leads to glucose intolerance and insulin resistance, which would generally limit its utility, especially in obese patients with prediabetes and diabetes.[19,75,76] We also found that, although not worsening diabetes, RAP treatment of DIO mice has only a marginal effect on improving glucose metabolism in DIO mice. It seems likely that the benefit of weight loss is counteracted by the negative effect of RAP on insulin signaling. Consistent with this, we found that co-administration of RAP and LEP significantly ameliorated glucose intolerance in WT mice but not in mice with defects in melanocortin signaling. This is consistent with prior studies showing that LEP improves glucose tolerance in mice with mutations in *Akt* and that POMC neurons have effects on glucose metabolism independent of their effects on body weight.[23,65,79–81]

Although several new incretin-based therapies have shown potent effects on reversing obesity, it is likely that other therapeutic approaches will be necessary for managing obesity in patients who cannot tolerate these drugs or fail to respond to them, or to help maintain weight in patients after treatment.[82,83] Overall, these data suggest that selective inhibition of mTOR in POMC neurons could provide an alternative therapeutic strategy. The development of brain-specific rapalogs provides a possible means to selectively reduce mTOR activity in the brain, and it might also be possible to develop cell-specific mTOR modulators.[84–87] Alternatively, the development of means for cell-specific delivery of RAP to POMC neurons could provide new avenues for treating obesity or maintaining weight loss.

In summary, we show that LEP resistance in DIO animals is caused by increased mTOR activity in POMC neurons and that RAP reduces obesity by re-sensitizing endogenous LEP signaling in these cells. These findings thus have important implications for our understanding of the pathogenesis of obesity and potential therapeutic applications.

Limitations of the study

Although our data show that increased mTOR activity in POMC neurons contributes to LEP resistance in DIO animals, it is not clear why feeding mice a HFD increases mTOR activity in neurons. Further experiments to probe the mechanisms by which mTOR is activated in DIO mice will be necessary. In addition, although our single-cell sequencing data in the ARC suggest that short-term RAP treatment primarily affects POMC neurons, it is possible that other cell types in the hypothalamus or elsewhere might also contribute. These other cell types might be direct targets or connect to POMC neurons at the circuit level to regulate their intracellular mTOR activity. Alternatively, these other sites could act independently of POMC neurons, and the identification of these other potential targets will be necessary. Finally, the use of RAP as a LEP sensitizer for the treatment of obesity should be approached with caution, as RAP also affects glucose tolerance, lean mass, and possibly other pathways. Efforts to develop cell-type-specific means for reducing mTOR activity to increase LEP sensitivity may thus represent a novel therapeutic approach, but it will be important to minimize effects on mTOR activity elsewhere.

RESOURCE AVAILABILITY

Lead contact

Further information and requests for resources and reagents should be directed to the lead contact, Dr. Jeffrey M. Friedman (friedj@rockefeller.edu).

Materials availability

All reagents generated in this study will be made available on request, pending a completed materials transfer agreement. Reimbursement for associated expenses may be requested, depending on the cost.

Data and code availability

- Source data are available in Data S1.
- The snRNA sequencing data generated in this study have been submitted to the NCBI Gene Expression Omnibus (GEO: GSE281687).
- This paper does not report original code.
- Any additional information reported in this work is available from the lead contact upon request.

ACKNOWLEDGMENTS

We thank Cori Bargmann and Nat Heintz for their input. We thank Liza Reizis for help with histology and genotyping, Donghoon Lee for help with tissue dissections, and Lisa Pomeranz and Max Halaas for help with pair-feeding animals. We thank Hector Lugo for care of animals. We thank Xianfeng Zeng and Wenyun Lu for assisting Z.Z. with sample preparation, lipidomics analysis, and developing the liquid chromatography (LC) methods. We thank Connie Zhao and Hong Duan for help with 10x Genomics library preparation and sequencing. B.T. acknowledges support from the David Rockefeller Fellowship. J.M.F. acknowledges support from the JPB Foundation. B.T. and K.H. acknowledge support from the Robertson Therapeutic Development Fund and the clinical and translational science awards.

AUTHOR CONTRIBUTIONS

B.T. conceived and led the study, designed and conducted the experiments, analyzed the data, conceptualized the results, and wrote the manuscript. K.H. designed and conducted the experiments, analyzed the data, bred mouse models, wrote the manuscript, and conceptualized the results. L.K. conducted electrophysiological recordings and analysis. A.M.-A. conducted and analyzed histology data for the revised manuscript. J.-D.L. conducted quality control and initial analysis of snRNA-seq datasets. Z.Z. conducted metabolomic and lipidomic sample preparation and analysis. J.D.R. provided resources for metabolomics and lipidomics and contributed to the analysis. J.M.F. conceived and led the study, wrote the manuscript, and conceptualized the results.

DECLARATION OF INTERESTS

J.M.F. is listed on a patent for the use of LEP (metreleptin) for the treatment of lipodystrophy and, as per Rockefeller University policy, receives a portion of the royalties from its sale.

STAR★METHODS

Detailed methods are provided in the online version of this paper and include the following:

- KEY RESOURCES TABLE
- EXPERIMENTAL MODEL AND STUDY PARTICIPANT DETAILS
  - Animals
- METHOD DETAILS
  - Plasma metabolomics and lipidomics
  - Pharmacological administration
  - Magnetic resonance imaging (MRI)
  - Leptin sensitivity test
  - Glucose tolerance test

SUPPLEMENTAL INFORMATION

Supplemental information can be found online at https://doi.org/10.1016/j.cmet.2025.01.001.

Received: November 13, 2023
Revised: September 9, 2024
Accepted: January 2, 2025
Published: March 4, 2025

REFERENCES

1. The Lancet Gastroenterology, H. (2021). Obesity: another ongoing pandemic. Lancet Gastroenterol. Hepatol. *6*, 411. https://doi.org/10.1016/S2468-1253(21)00143-6.
2. Halaas, J.L., Gajiwala, K.S., Maffei, M., Cohen, S.L., Chait, B.T., Rabinowitz, D., Lallone, R.L., Burley, S.K., and Friedman, J.M. (1995). Weight-reducing effects of the plasma protein encoded by the obese gene. Science *269*, 543–546. https://doi.org/10.1126/science.7624777.
3. Halaas, J.L., Boozer, C., Blair-West, J., Fidahusein, N., Denton, D.A., and Friedman, J.M. (1997). Physiological response to long-term peripheral and central leptin infusion in lean and obese mice. Proc. Natl. Acad. Sci. USA *94*, 8878–8883. https://doi.org/10.1073/pnas.94.16.8878.
4. Liu, H., He, Y., Bai, J., Zhang, C., Zhang, F., Yang, Y., Luo, H., Yu, M., Liu, H., Tu, L., et al. (2023). Hypothalamic Grb10 enhances leptin signalling and promotes weight loss. Nat. Metab. *5*, 147–164. https://doi.org/10.1038/s42255-022-00701-x.
5. Xu, A.W., Ste-Marie, L., Kaelin, C.B., and Barsh, G.S. (2007). Inactivation of signal transducer and activator of transcription 3 in proopiomelanocortin (Pomc) neurons causes decreased POMC expression, mild obesity, and defects in compensatory refeeding. Endocrinology *148*, 72–80. https://doi.org/10.1210/en.2006-1119.
6. Cowley, M.A., Smart, J.L., Rubinstein, M., Cerdán, M.G., Diano, S., Horvath, T.L., Cone, R.D., and Low, M.J. (2001). Leptin activates anorexigenic POMC neurons through a neural network in the arcuate nucleus. Nature *411*, 480–484. https://doi.org/10.1038/35078085.
7. Maffei, M., Halaas, J., Ravussin, E., Pratley, R.E., Lee, G.H., Zhang, Y., Fei, H., Kim, S., Lallone, R., and Ranganathan, S. (1995). Leptin levels in human and rodent: measurement of plasma leptin and Ob RNA in obese and weight-reduced subjects. Nat. Med. *1*, 1155–1161. https://doi.org/10.1038/nm1195-1155.
8. Heymsfield, S.B., Greenberg, A.S., Fujioka, K., Dixon, R.M., Kushner, R., Hunt, T., Lubina, J.A., Patane, J., Self, B., Hunt, P., et al. (1999). Recombinant leptin for weight loss in obese and lean adults: a randomized, controlled, dose-escalation trial. JAMA *282*, 1568–1575. https://doi.org/10.1001/jama.282.16.1568.
9. Christoffersen, B.Ø., Sanchez-Delgado, G., John, L.M., Ryan, D.H., Raun, K., and Ravussin, E. (2022). Beyond appetite regulation: targeting energy expenditure, fat oxidation, and lean mass preservation for sustainable weight loss. Obesity (Silver Spring) *30*, 841–857. https://doi.org/10.1002/oby.23374.
10. Lawler, K., Huang-Doran, I., Sonoyama, T., Collet, T.H., Keogh, J.M., Henning, E., O'rahilly, S., Bottolo, L., and Farooqi, I.S. (2020). Leptin-mediated changes in the human metabolome. J. Clin. Endocrinol. Metab. *105*, 2541–2552. https://doi.org/10.1210/clinem/dgaa251.
11. Wolfson, R.L., Chantranupong, L., Saxton, R.A., Shen, K., Scaria, S.M., Cantor, J.R., and Sabatini, D.M. (2016). Sestrin2 is a leucine sensor for the mTORC1 pathway. Science *351*, 43–48. https://doi.org/10.1126/science.aab2674.
12. Gu, X., Orozco, J.M., Saxton, R.A., Condon, K.J., Liu, G.Y., Krawczyk, P.A., Scaria, S.M., Harper, J.W., Gygi, S.P., and Sabatini, D.M. (2017). SAMTOR is an S-adenosylmethionine sensor for the mTORC1 pathway. Science *358*, 813–818. https://doi.org/10.1126/science.aao3265.
13. Laplante, M., and Sabatini, D.M. (2009). An emerging role of mTOR in lipid biosynthesis. Curr. Biol. *19*, R1046–R1052. https://doi.org/10.1016/j.cub.2009.09.058.
14. Drummond, M.J., Fry, C.S., Glynn, E.L., Dreyer, H.C., Dhanani, S., Timmerman, K.L., Volpi, E., and Rasmussen, B.B. (2009). Rapamycin administration in humans blocks the contraction-induced increase in skeletal muscle protein synthesis. J. Physiol. *587*, 1535–1546. https://doi.org/10.1113/jphysiol.2008.163816.
15. Yoon, M.S. (2017). mTOR as a key regulator in maintaining skeletal muscle Mass. Front. Physiol. *8*, 788. https://doi.org/10.3389/fphys.2017.00788.
16. Shi, H., Akunuru, S., Bierman, J.C., Hodge, K.M., Mitchell, M.C., Foster, M.T., Seeley, R.J., and Reizes, O. (2009). Diet-induced obese mice are leptin insufficient after weight reduction. Obesity (Silver Spring) *17*, 1702–1709. https://doi.org/10.1038/oby.2009.106.
17. Levin, B.E., and Dunn-Meynell, A.A. (2002). Defense of body weight depends on dietary composition and palatability in rats with diet-induced obesity. Am. J. Physiol. Regul. Integr. Comp. Physiol. *282*, R46–R54. https://doi.org/10.1152/ajpregu.2002.282.1.R46.
18. Chellappa, K., Perron, I.J., Naidoo, N., and Baur, J.A. (2019). The leptin sensitizer celastrol reduces age-associated obesity and modulates behavioral rhythms. Aging Cell *18*, e12874. https://doi.org/10.1111/acel.12874.
19. Kocalis, H.E., Hagan, S.L., George, L., Turney, M.K., Siuta, M.A., Laryea, G.N., Morris, L.C., Muglia, L.J., Printz, R.L., Stanwood, G.D., et al. (2014). Rictor/mTORC2 facilitates central regulation of energy and glucose homeostasis. Mol. Metab. *3*, 394–407. https://doi.org/10.1016/j.molmet.2014.01.014.
20. Kamohara, S., Burcelin, R., Halaas, J.L., Friedman, J.M., and Charron, M.J. (1997). Acute stimulation of glucose metabolism in mice by leptin treatment. Nature *389*, 374–377. https://doi.org/10.1038/38717.
21. Park, Y.G., Sohn, C.H., Chen, R., McCue, M., Yun, D.H., Drummond, G.T., Ku, T., Evans, N.B., Oak, H.C., Trieu, W., et al. (2018). Protection of tissue physicochemical properties using polyfunctional crosslinkers. Nat. Biotechnol. https://doi.org/10.1038/nbt.4281.
22. Friedman, J.M. (2019). Leptin and the endocrine control of energy balance. Nat. Metab. *1*, 754–764. https://doi.org/10.1038/s42255-019-0095-y.
23. Xu, J., Bartolome, C.L., Low, C.S., Yi, X., Chien, C.H., Wang, P., and Kong, D. (2018). Genetic identification of leptin neural circuits in energy and glucose homeostases. Nature *556*, 505–509. https://doi.org/10.1038/s41586-018-0049-7.
24. Campbell, J.N., Macosko, E.Z., Fenselau, H., Pers, T.H., Lyubetskaya, A., Tenen, D., Goldman, M., Verstegen, A.M.J., Resch, J.M., McCarroll, S.A., et al. (2017). A molecular census of arcuate hypothalamus and median eminence cell types. Nat. Neurosci. *20*, 484–496. https://doi.org/10.1038/nn.4495.
25. Biglari, N., Gaziano, I., Schumacher, J., Radermacher, J., Paeger, L., Klemm, P., Chen, W., Corneliussen, S., Wunderlich, C.M., Sue, M., et al. (2021). Functionally distinct POMC-expressing neuron subpopulations in hypothalamus revealed by intersectional targeting. Nat. Neurosci. *24*, 913–929. https://doi.org/10.1038/s41593-021-00854-0.
26. Deng, G., Morselli, L.L., Wagner, V.A., Balapattabi, K., Sapouckey, S.A., Knudtson, K.L., Rahmouni, K., Cui, H., Sigmund, C.D., Kwitek, A.E., et al. (2020). Single-nucleus RNA sequencing of the hypothalamic arcuate nucleus of C57BL/6J mice after prolonged diet-induced obesity.

Hypertension *76*, 589–597. https://doi.org/10.1161/HYPERTENSIONAHA.120.15137.

27. Saucisse, N., Mazier, W., Simon, V., Binder, E., Catania, C., Bellocchio, L., Romanov, R.A., Léon, S., Matias, I., Zizzari, P., et al. (2021). Functional heterogeneity of POMC neurons relies on mTORC1 signaling. Cell Rep. *37*, 109800. https://doi.org/10.1016/j.celrep.2021.109800.

28. Steuernagel, L., Lam, B.Y.H., Klemm, P., Dowsett, G.K.C., Bauder, C.A., Tadross, J.A., Hitschfeld, T.S., Del Rio Martin, A., Chen, W., de Solis, A.J., et al. (2022). HypoMap-a unified single-cell gene expression atlas of the murine hypothalamus. Nat. Metab. *4*, 1402–1419. https://doi.org/10.1038/s42255-022-00657-y.

29. Zhang, X., Guo, A., Yu, J., Possemato, A., Chen, Y., Zheng, W., Polakiewicz, R.D., Kinzler, K.W., Vogelstein, B., Velculescu, V.E., et al. (2007). Identification of STAT3 as a substrate of receptor protein tyrosine phosphatase T. Proc. Natl. Acad. Sci. USA *104*, 4060–4064. https://doi.org/10.1073/pnas.0611665104.

30. Pei, Z., He, Y., Bean, J.C., Yang, Y., Liu, H., Yu, M., Yu, K., Hyseni, I., Cai, X., Liu, H., et al. (2022). Gabra5 plays a sexually dimorphic role in POMC neuron activity and glucose balance. Front. Endocrinol. (Lausanne) *13*, 889122. https://doi.org/10.3389/fendo.2022.889122.

31. Vong, L., Ye, C., Yang, Z., Choi, B., Chua, S., Jr., and Lowell, B.B. (2011). Leptin action on GABAergic neurons prevents obesity and reduces inhibitory tone to POMC neurons. Neuron *71*, 142–154. https://doi.org/10.1016/j.neuron.2011.05.028.

32. Zhan, C., Zhou, J., Feng, Q., Zhang, J.E., Lin, S., Bao, J., Wu, P., and Luo, M. (2013). Acute and long-term suppression of feeding behavior by POMC neurons in the brainstem and hypothalamus, respectively. J. Neurosci. *33*, 3624–3632. https://doi.org/10.1523/JNEUROSCI.2742-12.2013.

33. Loos, R.J.F., Lindgren, C.M., Li, S., Wheeler, E., Zhao, J.H., Prokopenko, I., Inouye, M., Freathy, R.M., Attwood, A.P., Beckmann, J.S., et al. (2008). Common variants near MC4R are associated with fat mass, weight and risk of obesity. Nat. Genet. *40*, 768–775. https://doi.org/10.1038/ng.140.

34. Yang, S.B., Tien, A.C., Boddupalli, G., Xu, A.W., Jan, Y.N., and Jan, L.Y. (2012). Rapamycin ameliorates age-dependent obesity associated with increased mTOR signaling in hypothalamic POMC neurons. Neuron *75*, 425–436. https://doi.org/10.1016/j.neuron.2012.03.043.

35. Mori, H., Inoki, K., Münzberg, H., Opland, D., Faouzi, M., Villanueva, E.C., Ikenoue, T., Kwiatkowski, D., MacDougald, O.A., Myers, M.G., Jr., et al. (2009). Critical role for hypothalamic mTOR activity in energy balance. Cell Metab. *9*, 362–374. https://doi.org/10.1016/j.cmet.2009.03.005.

36. Valenstein, M.L., Rogala, K.B., Lalgudi, P.V., Brignole, E.J., Gu, X., Saxton, R.A., Chantranupong, L., Kolibius, J., Quast, J.P., and Sabatini, D.M. (2022). Structure of the nutrient-sensing hub GATOR2. Nature *607*, 610–616. https://doi.org/10.1038/s41586-022-04939-z.

37. Cai, W., Wei, Y., Jarnik, M., Reich, J., and Lilly, M.A. (2016). The GATOR2 component Wdr24 regulates TORC1 activity and lysosome function. PLoS Genet. *12*, e1006036. https://doi.org/10.1371/journal.pgen.1006036.

38. Yang, H., Jiang, X., Li, B., Yang, H.J., Miller, M., Yang, A., Dhar, A., and Pavletich, N.P. (2017). Mechanisms of mTORC1 activation by RHEB and inhibition by PRAS40. Nature *552*, 368–373. https://doi.org/10.1038/nature25023.

39. Inoki, K., Li, Y., Xu, T., and Guan, K.L. (2003). Rheb GTPase is a direct target of TSC2 GAP activity and regulates mTOR signaling. Genes Dev. *17*, 1829–1834. https://doi.org/10.1101/gad.1110003.

40. Frank, G.R., Fox, J., Candela, N., Jovanovic, Z., Bochukova, E., Levine, J., Papenhausen, P.R., O'Rahilly, S., and Farooqi, I.S. (2013). Severe obesity and diabetes insipidus in a patient with PCSK1 deficiency. Mol. Genet. Metab. *110*, 191–194. https://doi.org/10.1016/j.ymgme.2013.04.005.

41. Fenselau, H., Campbell, J.N., Verstegen, A.M.J., Madara, J.C., Xu, J., Shah, B.P., Resch, J.M., Yang, Z., Mandelblat-Cerf, Y., Livneh, Y., et al. (2017). A rapidly acting glutamatergic ARC–>PVH satiety circuit postsynaptically regulated by alpha-MSH. Nat. Neurosci. *20*, 42–51. https://doi.org/10.1038/nn.4442.

42. Yaswen, L., Diehl, N., Brennan, M.B., and Hochgeschwender, U. (1999). Obesity in the mouse model of pro-opiomelanocortin deficiency responds to peripheral melanocortin. Nat. Med. *5*, 1066–1070. https://doi.org/10.1038/12506.

43. Kievit, P., Halem, H., Marks, D.L., Dong, J.Z., Glavas, M.M., Sinnayah, P., Pranger, L., Cowley, M.A., Grove, K.L., and Culler, M.D. (2013). Chronic treatment with a melanocortin-4 receptor agonist causes weight loss, reduces insulin resistance, and improves cardiovascular function in diet-induced obese rhesus macaques. Diabetes *62*, 490–497. https://doi.org/10.2337/db12-0598.

44. Chen, K.Y., Muniyappa, R., Abel, B.S., Mullins, K.P., Staker, P., Brychta, R.J., Zhao, X., Ring, M., Psota, T.L., Cone, R.D., et al. (2015). RM-493, a melanocortin-4 receptor (MC4R) agonist, increases resting energy expenditure in obese individuals. J. Clin. Endocrinol. Metab. *100*, 1639–1645. https://doi.org/10.1210/jc.2014-4024.

45. Knight, Z.A., Hannan, K.S., Greenberg, M.L., and Friedman, J.M. (2010). Hyperleptinemia is required for the development of leptin resistance. PLoS One *5*, e11376. https://doi.org/10.1371/journal.pone.0011376.

46. Zhao, S., Zhu, Y., Schultz, R.D., Li, N., He, Z., Zhang, Z., Caron, A., Zhu, Q., Sun, K., Xiong, W., et al. (2019). Partial leptin reduction as an insulin sensitization and weight loss strategy. Cell Metab. *30*, 706–719.e6. https://doi.org/10.1016/j.cmet.2019.08.005.

47. Ottaway, N., Mahbod, P., Rivero, B., Norman, L.A., Gertler, A., D'Alessio, D.A., and Perez-Tilve, D. (2015). Diet-induced obese mice retain endogenous leptin action. Cell Metab. *21*, 877–882. https://doi.org/10.1016/j.cmet.2015.04.015.

48. Shanik, M.H., Xu, Y., Skrha, J., Dankner, R., Zick, Y., and Roth, J. (2008). Insulin resistance and hyperinsulinemia: is hyperinsulinemia the cart or the horse? Diabetes Care *31*, S262–S268. https://doi.org/10.2337/dc08-s264.

49. Wang, L., Ren, B., Zhang, Q., Chu, C., Zhao, Z., Wu, J., Zhao, W., Liu, Z., and Liu, X. (2020). Methionine restriction alleviates high-fat diet-induced obesity: involvement of diurnal metabolism of lipids and bile acids. Biochim. Biophys. Acta Mol. Basis Dis. *1866*, 165908. https://doi.org/10.1016/j.bbadis.2020.165908.

50. Zhou, Z., Yin, H., Guo, Y., Fang, Y., Yuan, F., Chen, S., and Guo, F. (2021). A fifty percent leucine-restricted diet reduces fat mass and improves glucose regulation. Nutr. Metab. (Lond.) *18*, 34. https://doi.org/10.1186/s12986-021-00564-1.

51. Zhang, Q., Liu, B., Cheng, Y., Meng, Q., Xia, T., Jiang, L., Chen, S., Liu, Y., and Guo, F. (2014). Leptin signaling is required for leucine deprivation-enhanced energy expenditure. J. Biol. Chem. *289*, 1779–1787. https://doi.org/10.1074/jbc.M113.528943.

52. Cota, D., Proulx, K., Smith, K.A.B., Kozma, S.C., Thomas, G., Woods, S.C., and Seeley, R.J. (2006). Hypothalamic mTOR signaling regulates food intake. Science *312*, 927–930. https://doi.org/10.1126/science.1124147.

53. Ernst, M.B., Wunderlich, C.M., Hess, S., Paehler, M., Mesaros, A., Koralov, S.B., Kleinridders, A., Husch, A., Münzberg, H., Hampel, B., et al. (2009). Enhanced Stat3 activation in POMC neurons provokes negative feedback inhibition of leptin and insulin signaling in obesity. J. Neurosci. *29*, 11582–11593. https://doi.org/10.1523/JNEUROSCI.5712-08.2009.

54. Pedroso, J.A.B., Buonfiglio, D.C., Cardinali, L.I., Furigo, I.C., Ramos-Lobo, A.M., Tirapegui, J., Elias, C.F., and Donato, J., Jr. (2014). Inactivation of SOCS3 in leptin receptor-expressing cells protects mice from diet-induced insulin resistance but does not prevent obesity. Mol. Metab. *3*, 608–618. https://doi.org/10.1016/j.molmet.2014.06.001.

55. Olofsson, L.E., Unger, E.K., Cheung, C.C., and Xu, A.W. (2013). Modulation of AgRP-neuronal function by SOCS3 as an initiating event in diet-induced hypothalamic leptin resistance. Proc. Natl. Acad. Sci. USA *110*, E697–E706. https://doi.org/10.1073/pnas.1218284110.

56. Howard, J.K., Cave, B.J., Oksanen, L.J., Tzameli, I., Bjørbaek, C., and Flier, J.S. (2004). Enhanced leptin sensitivity and attenuation of

diet-induced obesity in mice with haploinsufficiency of Socs3. Nat. Med. *10*, 734–738. https://doi.org/10.1038/nm1072.

57. Mori, H., Hanada, R., Hanada, T., Aki, D., Mashima, R., Nishinakamura, H., Torisu, T., Chien, K.R., Yasukawa, H., and Yoshimura, A. (2004). Socs3 deficiency in the brain elevates leptin sensitivity and confers resistance to diet-induced obesity. Nat. Med. *10*, 739–743. https://doi.org/10.1038/nm1071.
58. Bjorbak, C., Lavery, H.J., Bates, S.H., Olson, R.K., Davis, S.M., Flier, J.S., and Myers, M.G., Jr. (2000). SOCS3 mediates feedback inhibition of the leptin receptor via Tyr985. J. Biol. Chem. *275*, 40649–40657. https://doi.org/10.1074/jbc.M007577200.
59. Bence, K.K., Delibegovic, M., Xue, B., Gorgun, C.Z., Hotamisligil, G.S., Neel, B.G., and Kahn, B.B. (2006). Neuronal PTP1B regulates body weight, adiposity and leptin action. Nat. Med. *12*, 917–924. https://doi.org/10.1038/nm1435.
60. Cheng, A., Uetani, N., Simoncic, P.D., Chaubey, V.P., Lee-Loy, A., McGlade, C.J., Kennedy, B.P., and Tremblay, M.L. (2002). Attenuation of leptin action and regulation of obesity by protein tyrosine phosphatase 1B. Dev. Cell *2*, 497–503. https://doi.org/10.1016/s1534-5807(02)00149-1.
61. Plum, L., Ma, X., Hampel, B., Balthasar, N., Coppari, R., Münzberg, H., Shanabrough, M., Burdakov, D., Rother, E., Janoschek, R., et al. (2006). Enhanced PIP3 signaling in POMC neurons causes KATP channel activation and leads to diet-sensitive obesity. J. Clin. Invest. *116*, 1886–1901. https://doi.org/10.1172/JCI27123.
62. Yu, Y., Yoon, S.O., Poulogiannis, G., Yang, Q., Ma, X.M., Villén, J., Kubica, N., Hoffman, G.R., Cantley, L.C., Gygi, S.P., et al. (2011). Phosphoproteomic analysis identifies Grb10 as an mTORC1 substrate that negatively regulates insulin signaling. Science *332*, 1322–1326. https://doi.org/10.1126/science.1199484.
63. Çakır, I., Hadley, C.K., Pan, P.L., Bagchi, R.A., Ghamari-Langroudi, M., Porter, D.T., Wang, Q., Litt, M.J., Jana, S., Hagen, S., et al. (2022). Histone deacetylase 6 inhibition restores leptin sensitivity and reduces obesity. Nat. Metab. *4*, 44–59. https://doi.org/10.1038/s42255-021-00515-3.
64. Park, S., Aintablian, A., Coupe, B., and Bouret, S.G. (2020). The endoplasmic reticulum stress-autophagy pathway controls hypothalamic development and energy balance regulation in leptin-deficient neonates. Nat. Commun. *11*, 1914. https://doi.org/10.1038/s41467-020-15624-y.
65. Coupé, B., Ishii, Y., Dietrich, M.O., Komatsu, M., Horvath, T.L., and Bouret, S.G. (2012). Loss of autophagy in pro-opiomelanocortin neurons perturbs axon growth and causes metabolic dysregulation. Cell Metab. *15*, 247–255. https://doi.org/10.1016/j.cmet.2011.12.016.
66. Suyama, S., Ralevski, A., Liu, Z.W., Dietrich, M.O., Yada, T., Simonds, S.E., Cowley, M.A., Gao, X.B., Diano, S., and Horvath, T.L. (2017). Plasticity of calcium-permeable AMPA glutamate receptors in pro-opiomelanocortin neurons. eLife *6*, e25755. https://doi.org/10.7554/eLife.25755.
67. Diano, S., Liu, Z.W., Jeong, J.K., Dietrich, M.O., Ruan, H.B., Kim, E., Suyama, S., Kelly, K., Gyengesi, E., Arbiser, J.L., et al. (2011). Peroxisome proliferation-associated control of reactive oxygen species sets melanocortin tone and feeding in diet-induced obesity. Nat. Med. *17*, 1121–1127. https://doi.org/10.1038/nm.2421.
68. Schneeberger, M., Dietrich, M.O., Sebastián, D., Imbernón, M., Castaño, C., Garcia, A., Esteban, Y., Gonzalez-Franquesa, A., Rodríguez, I.C., Bortolozzi, A., et al. (2013). Mitofusin 2 in POMC neurons connects ER stress with leptin resistance and energy imbalance. Cell *155*, 172–187. https://doi.org/10.1016/j.cell.2013.09.003.
69. Ozcan, L., Ergin, A.S., Lu, A., Chung, J., Sarkar, S., Nie, D., Myers, M.G., Jr., and Ozcan, U. (2009). Endoplasmic reticulum stress plays a central role in development of leptin resistance. Cell Metab. *9*, 35–51. https://doi.org/10.1016/j.cmet.2008.12.004.
70. Feng, X., Guan, D., Auen, T., Choi, J.W., Salazar Hernández, M.A., Lee, J., Chun, H., Faruk, F., Kaplun, E., Herbert, Z., et al. (2019). IL1R1 is required for celastrol's leptin-sensitization and antiobesity effects. Nat. Med. *25*, 575–582. https://doi.org/10.1038/s41591-019-0358-x.
71. Lee, J., Liu, J., Feng, X., Salazar Hernández, M.A., Mucka, P., Ibi, D., Choi, J.W., and Ozcan, U. (2016). Withaferin A is a leptin sensitizer with strong antidiabetic properties in mice. Nat. Med. *22*, 1023–1032. https://doi.org/10.1038/nm.4145.
72. Liu, J., Lee, J., Salazar Hernandez, M.A., Mazitschek, R., and Ozcan, U. (2015). Treatment of obesity with celastrol. Cell *161*, 999–1011. https://doi.org/10.1016/j.cell.2015.05.011.
73. Roth, J.D., Roland, B.L., Cole, R.L., Trevaskis, J.L., Weyer, C., Koda, J.E., Anderson, C.M., Parkes, D.G., and Baron, A.D. (2008). Leptin responsiveness restored by amylin agonism in diet-induced obesity: evidence from nonclinical and clinical studies. Proc. Natl. Acad. Sci. USA *105*, 7257–7262. https://doi.org/10.1073/pnas.0706473105.
74. Breit, S.N., Manandhar, R., Zhang, H.P., Lee-Ng, M., Brown, D.A., and Tsai, V.W.W. (2023). GDF15 enhances body weight and adiposity reduction in obese mice by leveraging the leptin pathway. Cell Metab. *35*, 1341–1355.e3. https://doi.org/10.1016/j.cmet.2023.06.009.
75. Saxton, R.A., and Sabatini, D.M. (2017). MTOR signaling in growth, metabolism, and disease. Cell *168*, 960–976. https://doi.org/10.1016/j.cell.2017.02.004.
76. Wullschleger, S., Loewith, R., and Hall, M.N. (2006). TOR signaling in growth and metabolism. Cell *124*, 471–484. https://doi.org/10.1016/j.cell.2006.01.016.
77. Harrison, D.E., Strong, R., Sharp, Z.D., Nelson, J.F., Astle, C.M., Flurkey, K., Nadon, N.L., Wilkinson, J.E., Frenkel, K., Carter, C.S., et al. (2009). Rapamycin fed late in life extends lifespan in genetically heterogeneous mice. Nature *460*, 392–395. https://doi.org/10.1038/nature08221.
78. Wormser, N., Di Angelantonio, E., Bhupathiraju, Sh.N., Wormser, D., Gao, P., Kaptoge, S., Berrington de Gonzalez, A., Cairns, B.J., Huxley, R., Jackson, Ch.L., et al. (2016). Body-mass index and all-cause mortality: individual-participant-data meta-analysis of 239 prospective studies in four continents. Lancet *388*, 776–786. https://doi.org/10.1016/S0140-6736(16)30175-1.
79. Hay, N. (2011). Akt isoforms and glucose homeostasis - the leptin connection. Trends Endocrinol. Metab. *22*, 66–73. https://doi.org/10.1016/j.tem.2010.09.003.
80. Chen, W.S., Peng, X.D., Wang, Y., Xu, P.Z., Chen, M.L., Luo, Y., Jeon, S.M., Coleman, K., Haschek, W.M., Bass, J., et al. (2009). Leptin deficiency and beta-cell dysfunction underlie type 2 diabetes in compound Akt knockout mice. Mol. Cell. Biol. *29*, 3151–3162. https://doi.org/10.1128/MCB.01792-08.
81. Parton, L.E., Ye, C.P., Coppari, R., Enriori, P.J., Choi, B., Zhang, C.Y., Xu, C., Vianna, C.R., Balthasar, N., Lee, C.E., et al. (2007). Glucose sensing by POMC neurons regulates glucose homeostasis and is impaired in obesity. Nature *449*, 228–232. https://doi.org/10.1038/nature06098.
82. Wilding, J.P.H., Batterham, R.L., Calanna, S., Davies, M., Van Gaal, L.F., Lingvay, I., McGowan, B.M., Rosenstock, J., Tran, M.T.D., Wadden, T.A., et al. (2021). Once-weekly semaglutide in adults with overweight or obesity. N. Engl. J. Med. *384*, 989–1002. https://doi.org/10.1056/NEJMoa2032183.
83. Jastreboff, A.M., Aronne, L.J., Ahmad, N.N., Wharton, S., Connery, L., Alves, B., Kiyosue, A., Zhang, S., Liu, B., Bunck, M.C., et al. (2022). Tirzepatide once weekly for the treatment of obesity. N. Engl. J. Med. *387*, 205–216. https://doi.org/10.1056/NEJMoa2206038.
84. Zhang, Z., Fan, Q., Luo, X., Lou, K., Weiss, W.A., and Shokat, K.M. (2022). Brain-restricted mTOR inhibition with binary pharmacology. Nature *609*, 822–828. https://doi.org/10.1038/s41586-022-05213-y.
85. Tan, B., Nöbauer, T., Browne, C.J., Nestler, E.J., Vaziri, A., and Friedman, J.M. (2022). Dynamic processing of hunger and thirst by common mesolimbic neural ensembles. Proc. Natl. Acad. Sci. USA *119*, e2211688119. https://doi.org/10.1073/pnas.2211688119.
86. Tan, B., Browne, C.J., Nöbauer, T., Vaziri, A., Friedman, J.M., and Nestler, E.J. (2023). Drugs of abuse hijack a mesolimbic pathway that processes

homeostatic need. Preprint at bioRxiv. https://doi.org/10.1101/2023.09.03.556059.

87. Tang, G., Gudsnuk, K., Kuo, S.H., Cotrina, M.L., Rosoklija, G., Sosunov, A., Sonders, M.S., Kanter, E., Castagna, C., Yamamoto, A., et al. (2014). Loss of mTOR-dependent macroautophagy causes autistic-like synaptic pruning deficits. Neuron *83*, 1131–1143. https://doi.org/10.1016/j.neuron.2014.07.040.

88. Wolock, S.L., Lopez, R., and Klein, A.M. (2019). Scrublet: computational identification of cell doublets in single-cell transcriptomic data. Cell Syst. *8*, 281–291.e9. https://doi.org/10.1016/j.cels.2018.11.005.

89. Young, M.D., and Behjati, S. (2020). SoupX removes ambient RNA contamination from droplet-based single-cell RNA sequencing data. GigaScience *9*, giaa151. https://doi.org/10.1093/gigascience/giaa151.

90. Stuart, T., Butler, A., Hoffman, P., Hafemeister, C., Papalexi, E., Mauck, W.M., 3rd, Hao, Y., Stoeckius, M., Smibert, P., and Satija, R. (2019). Comprehensive integration of single-cell data. Cell *177*, 1888–1902.e21. https://doi.org/10.1016/j.cell.2019.05.031.

91. Becht, E., McInnes, L., Healy, J., Dutertre, C.A., Kwok, I.W.H., Ng, L.G., Ginhoux, F., and Newell, E.W. (2018). Dimensionality reduction for visualizing single-cell data using UMAP. Nat. Biotechnol. https://doi.org/10.1038/nbt.4314.

92. Traag, V.A., Waltman, L., and van Eck, N.J. (2019). From Louvain to Leiden: guaranteeing well-connected communities. Sci. Rep. *9*, 5233. https://doi.org/10.1038/s41598-019-41695-z.

93. Negoescu, A., Labat-Moleur, F., Lorimier, P., Lamarcq, L., Guillermet, C., Chambaz, E., and Brambilla, E. (1994). F(ab) secondary antibodies: a general method for double immunolabeling with primary antisera from the same species. Efficiency control by chemiluminescence. J. Histochem. Cytochem. *42*, 433–437. https://doi.org/10.1177/42.3.7508473.

94. Secci, M.E., Reed, T., Quinlan, V., Gilpin, N.W., and Avegno, E.M. (2023). Quantitative analysis of gene expression in RNAscope-processed brain tissue. Bio Protoc. *13*, e4580. https://doi.org/10.21769/BioProtoc.4580.

95. Schwarzkopf, M., Liu, M.C., Schulte, S.J., Ives, R., Husain, N., Choi, H.M.T., and Pierce, N.A. (2021). Hybridization chain reaction enables a unified approach to multiplexed, quantitative, high-resolution immunohistochemistry and in situ hybridization. Development *148*, dev199847. https://doi.org/10.1242/dev.199847.

STAR★METHODS

KEY RESOURCES TABLE

REAGENT or RESOURCE	SOURCE	IDENTIFIER
Antibodies		
pSTAT3	Cell Signaling	Cat# 9145; RRID:AB_2491009
pS6	Thermo Fisher Scientific	Cat# 44-923G; RRID:AB_2533798
Anti-GFP	Abcam	Cat# ab13970; RRID:AB_300798
Donkey anti-Chicken IgG Alexa 488	Jackson ImmunoResearch Labs	Cat# 703-546-155; RRID:AB_2340376
Donkey anti-Rabbit IgG Alexa 594	Invitrogen	Cat# A21207; RRID:AB_141637
DAPI Fluoromount-G	Southern Biotech	Cat# 0100-20
AgRP	Phoenix Pharmaceuticals	Cat# H-003-57; RRID:AB_2313909
Donkey anti-Rabbit IgG (H+L) Alexa 594	Jackson ImmunoResearch Labs	Cat# 711-585-152; RRID:AB_2340621
anti-NeuN Alexa 647	Abcam	Cat# ab190565; RRID:AB_2732785
TotalSeqB anti-Nuclear Pore HashTag 1	BioLegend	Cat# 682235; RRID:AB_2892484
TotalSeqB anti-Nuclear Pore HashTag 2	BioLegend	Cat# 682237; RRID:AB_2892485
Bacterial and virus strains		
AAV5-hSyn-DIO-mCherry	Addgene	Cat# 50459-AAV5
AAV5-EF1a-mCherry-FLEX-dtA	Addgene; Janelia viral core	Cat# 58536
AAV5-gRNAs$_{Wdr24}$-hSyn-mCherry	Janelia viral core	N/A
AAV5-gRNAs$_{Rheb}$-hSyn-mCherry	Janelia viral core	N/A
AAV5-gRNAs$_{scramble}$-hSyn-FLEX-H2B-EGFP	Janelia viral core	N/A
Chemicals, peptides, and recombinant proteins		
DPBS	Gibco	Cat# 14190-144
Recombinant mouse leptin protein	R&D	Cat# 498-OB-05M
Rapamycin	LC Laboratories	Cat# 53123-88-9
IGEPAL® CA-630	Sigma-Aldrich	Cat# I8896
Hoechst 33342	ThermoFisher Scientific	Cat# H3570
Actinomycin D	Sigma-Aldrich	Cat# A1410
SUPERase·In™ RNase Inhibitor	ThermoFisher Scientific	Cat# AM2696
RNasin	Promega	Cat# N2615
Halt™ Protease and Phosphatase Inhibitor Cocktail	ThermoFisher Scientific	Cat# 78442
PBS	Fisher Scientific	Cat# BP39920
PFA	EMS	Cat# 15714-S
Bovine serum albumin	Sigma	Cat# A9647-500G
Donkey serum	Jackson ImmunoResearch	Cat# 017-000-121
Triton X-100	ThermoFisher Scientific	Cat# 85111
Isoflurane	Henry Schein	Cat# 11695-6776-2
Critical commercial assays		
Hight-fat diet (60 kcal% Fat)	Research Diets	Cat# D12492
Standard-chow diet	PicoLab® Rodent Diet	Cat# 205053
Subcutaneous osmotic pump	Alzet	Cat# 2002, 2004, or 2006
Insulin syringes	Beckton Dickinson	Cat# 324911
Breeze2 glucometer	Bayer SKU	UPC: 301931440010
Echo-MRITM 100H	EchoMRI, LL	N/A
EDTA coated capillaries	Drummond Scientific	Cat# 2-000-100-D
Leptin ELISA	Alpco	Cat# 22-LEPMS-E01

(*Continued on next page*)

Continued

REAGENT or RESOURCE	SOURCE	IDENTIFIER
Deposited data		
Raw and processed data for single cell RNA-seq	NCBI GEO	GEO: GSE281687
Raw values used to generate all graphs	This Paper	Data S1 – Source Data
Experimental models: Organisms/strains		
Mouse: Wild-type mice	Jackson Laboratory	Cat# 000664
Mouse: db/db mice	Jackson Laboratory	Cat# 000697
Mouse: Mc4r-/- mice	Jackson Laboratory	Cat# 032518
Mouse: POMC-Cre mice	Jackson Laboratory	Cat# 005965
Mouse: Tsc1 fl/fl mice	Jackson Laboratory	Cat# 005680
Mouse: AgRP-Cre mice	Jackson Laboratory	Cat# 012899
Mouse: LSL-Cas9	Jackson Laboratory	Cat# 026175
Mouse: POMC-EGFP	Jackson Laboratory	Cat# 009593
Mouse: ob/+	Jackson Laboratory	Cat# 000632
Recombinant DNA		
pAAV-mCherry-flex-dtA	Addgene	Cat# 58536
pAAV-gRNAs$_{Wdr24}$-hSyn-mCherry	This paper	N/A
pAAV-gRNAs$_{Rheb}$-hSyn-mCherry	This paper	N/A
pAAV-gRNAs$_{scramble}$-hSyn-FLEX-H2B-EGFP	This paper	N/A
Software and algorithms		
CalR	CalR	https://www.calrapp.org
GraphPad Prism 9	GraphPad Software	https://www.graphpad.com
IGOR Pro	Wavemetrics	https://www.wavemetrics.com
NeuroMatic	NeuroMatic	http://www.neuromatic.thinkrandom.com
Fiji	ImageJ	https://imagej.net/software/fiji
Cellranger v6.0.0	Cell Ranger	https://www.10xgenomics.com/support/software/cell-ranger/latest
Scrublet	Scrublet	https://github.com/swolock/scrublet
SoupX	SoupX	https://github.com/constantAmateur/SoupX
Seurat	Seurat	https://satijalab.org/seurat/articles/hashing_vignette.html

EXPERIMENTAL MODEL AND STUDY PARTICIPANT DETAILS

Animals

Wild-type mice (#000664), *db/db* mice (#000697), *mc4r-/-* (#032518), POMC-Cre (#005965) *Tsc1 fl/fl* (#005680), AgRP-Cre (#012899), LSL-Cas9 (#026175), POMC-EGFP (#009593) were acquired from Jackson Lab and *ob/ob* were F1, bred in lab, from a cross between male *ob/ob* and female *ob/+* (#000632). All crosses were bred in lab from the above animals. Animals were kept at ambient temperature (64°F and 79°F) and humidity-controlled housing with a 12hr light-dark cycle (lights on at 7am and off at 7pm) and on a standard-chow diet (PicoLab® Rodent Diet 205053) unless otherwise indicated. Diet-induced-obese (DIO) wild-type mice were fed on high-fat diet (HFD, Research Diets, Cat# D12492, Rodent Diet With 60 kcal% Fat) starting at ~6 weeks old and used for experiments starting at 24 weeks old (fed on HFD for at least 18 weeks). Aged wild-type mice (12-16 months old) and young wildtype mice (~8 weeks old) were acquired from Jackson Lab #000664. All experiments were conducted according to AAALAC approved animal protocols. Males were used throughout. Males and female animals were used in Figures 3I–3P, 6F–6Q, and 7H–7Q (see figure legends). All experiments were internally sex and age matched.

METHOD DETAILS

Plasma metabolomics and lipidomics

Wildtype animals (Jackson #000664) were fed either chow (PicoLab® Rodent Diet 205053) or high fat diet (HFD, Research Diets cat. #D12492 Rodent Diet With 60 kcal% Fat) starting at 6-9 weeks of age. *ob/ob* males, bred in lab as described above, were also fed either chow or HFD and pairfed to their wildtype counterparts. Food intake for the wildtype animals were measured weekly, divided by 7, and then fed in that amount daily to the pairfed *ob/ob* animals for 18 weeks. Despite this pairfeeding scheme, the *ob/ob* animals

gained more weight than their wild-type counterparts. After 18 weeks of daily pairfeeding, all animals were i.p. injected with PBS (Gibco, Cat# 14190-144) at 12hour intervals for 24hrs and blood was collected and processed as described below in section (Leptin ELISA). Following 5 days of recovery, the animals were i.p. injected with 12.5 mg/kg leptin, dissolved in PBS at 12hour intervals for 24hrs and blood was again collected. **(1) Metabolomics.** For polar metabolites, 10ul of serum was extracted with 40ul MeOH pre-cooled on dry ice. After vertexing, samples are left on dry ice for 5min then centrifuged at 16,000 X g for 10 min at 4°C. Supernatant was subjected to LC-MS analysis. Positive and Negative mode of metabolomics were run on a quadrupole-orbitrap mass spectrometer (Q Exactive, Thermo Fisher Scientific, San Jose, CA) coupled with hydrophilic interaction chromatography (HILIC) via electrospray ionization. LC separation was done with a XBridge BEH Amide column (2.1 mm x 150 mm x 2.5 mm particle size, 130 A° pore size; Waters, Milford, MA) using a gradient of solvent A (20 mM ammonium acetate, 20 mM ammounium hydroxide in95:5 water:acetonitrile, pH 9.45) and solvent B (acetonitrile). Flow rate was 150 mL/min. The LC gradient was: 0 min, 85% B;2 min, 85% B; 3 min, 80% B; 5 min, 80% B; 6 min, 75% B; 7 min, 75% B; 8 min, 70% B; 9 min, 70% B; 10 min, 50% B; 12 min,50% B; 13 min, 25% B; 16 min, 25% B; 18 min, 0% B; 23 min, 0% B; 24 min, 85% B. Injection volume was 5ul for all serum samples at the autosampler temperature of 5 °C. (2) Lipidomics. Serum lipidomic samples are extracted with ethyl acetate. Serum (4μl) was added to ethyl acetate (100μl) and centrifuged 16,000 X g for 10min, and the supernatant was collected. The same process was repeated, and supernatant is combined. The resulting extract was dried down and redissolved in 1:1:1 methanol:acetonitrile:2-propanol (200μl) before analysis by Q Exactive Plus mass spectrometer coupled to a Vanquish UHPLC system (Thermo Fisher Scientific) using positive and negative-mode electrospray ionization. The LC separation was achieved on an Agilent Poroshell 120 EC-C18 column (150 × 2.1mm, 2.7 μm particle size) at a flow rate of 150 μl min^{-1}. The gradient was 0minutes, 25% B; 2minutes, 25% B; 4minutes, 65% B; 16minutes, 100% B; 20minutes, 100% B; 21minutes, 25% B; 27minutes, 25% B. Solvent A is 1mM ammonium acetate + 0.2% acetic acid in water:methanol (90:10). Solvent B is 1mM ammonium acetate + 0.2% acetic acid in methanol:2-propanol (2:98).

Pharmacological administration

Recombinant mouse leptin (R&D 498-OB-05M) was reconstituted in PBS and injected intraperitoneally (i.p.) or delivered via a subcutaneous osmotic pump (Alzet Cat# 2002, 2004, or 2006). Osmotic pumps were filled using sterile techniques and calibrated using the manufacturer's instructions. They were inserted dorsally under the skin of an isoflurane-anesthetized mouse using sterile surgery techniques. Rapamycin (LC Laboratories, Cat# 53123-88-9) was first dissolved in DMSO at 200 mg/ml, then diluted in 5% PEG 400 and 5% Tween 80 (in PBS) to a final concentration of 0.5 mg/ml. i.p. injections were done at indicated concentrations using insulin syringes (Beckton Dickinson, Cat# 324911).

Magnetic resonance imaging (MRI)

Body fat mass was measured by MRI in live mice using an Echo-MRI™ 100H (EchoMRI, LL). Machine was calibrated before use. No sedation or anesthesia was used, as per company protocol, but the animals were acclimated to the MRI tube before measurement. Body fat percentage was calculated by dividing fat mass over total body mass. Lean mass was calculated by subtracting fat mass from total body mass. Total body mass was measured by a CGOLDENWALL high precision lab scale.

Leptin sensitivity test

Animals were administered leptin (at indicated doses) or PBS either by i.p. injections every 12 hours or via osmotic pumps implanted 1 day prior to the start of the experiment. Food intake and body weight were measured through the course of treatment as indicated.

Glucose tolerance test

Animals fasted overnight were i.p. injected 5-20% glucose dissolved in PBS as indicated in the figure legends. Total amount of glucose injected was based on lean mass (determined with EchoMRI as per above) times the dosage. Dosage used for each experiment and cohort was indicated in the manuscript. Blood glucose in the GTT assay and *ad libitum*-fed conditions were measured by tail vein sampling using a Breeze2 glucometer (Bayer SKU: breeze2meter UPC: 301931440010). For the GTT in DIO mice in Figures S4G and S4H, the groups of mice receiving 600 ng/hr leptin (RAP+LEP and LEP) were i.p. injected 1 mg/kg leptin 1 hour prior to the glucose injection, while the other groups of mice (RAP and VEH) were i.p. injected PBS 1 hour prior to the GTT started.

Leptin ELISA

Blood (75-150 μl) was collected retro-orbitally at the indicated times in the manuscript using EDTA coated capillaries (Drummond Calibrated Micropipettes Glass Capillaries with EDTA 100μl, Cat# 2-000-100-D). Blood samples were spun for 20 minutes at 4°C and supernatant collected as plasma and frozen immediately in liquid nitrogen and stored at -80°C in screw cap tubes (Thermo Cat# 374503). Plasma leptin was measured by ELISA (Alpco, Cat# 22-LEPMS-E01) according to the manufacturer's protocol.

Pairfeeding or Pairfat conditions

Pairfeeding was conducted by measuring the daily or weekly food intake of the group which shows lower food intake and feeding that same amount to the other group. In some conditions where the group being pairfed still weighs significantly higher than the group it is pairfed to, we further restricted their food intake 10% lower than the amount of food they received in order to reach equal body weight (Pairfat) as the other group before the subsequent tests. Animals were single housed during experiments. Food intake and body

weight were measured daily or weekly using an Ohaus Scale. For pairfeeding in Figure 1, pairfeeding was done daily; however the amount fed was determined by measuring the food intake of the WTs once a week and dividing that by 7 and then feeding the OB animals that amount daily in the following week. For Figures 2I–2L, during weeks 19-23 (21 days), vehicle treated animals were fed, daily, what the rapamycin treated animals had eaten the preceding 24hours. For Figures 6K–6Q, animals were pairfed on HFD, food amount determined weekly in the first 16 weeks with the *mc4r-/-* cages receiving 10% less food than consumed by the wildtype animals. The last 3 weeks, animals were single housed and the *mc4r-/-* animals were precisely pairfed individually on a daily basis 10% less than what the wildtype animals were eating. This resulted in all groups weighing the same at the beginning of the ensuing leptin sensitivity tests. We refer to this protocol as ''Pairfat.'' For Figure 7E, animals were ''pairfat''-fed from 8 weeks of age.

Whole-brain mTOR activity (pS6) mapping

SHIELD-based whole-brain clearing and labeling was employed for mapping pS6 activity in DIO mice and chow fed mice. Mice *ad libitum* fed on HFD or chow were anesthetized with isoflurane and transcardially perfused with PBS containing 10 U/ml heparin, followed by 4% PFA. The dissected brains were fixed in 4% PFA for 24 h at 4 °C. Brains were then transferred to PBS containing 0.1% sodium azide until brain clearing and labeling. Brains were processed by LifeCanvas Technologies following the SHIELD protocol, as previously published and outlined on the LifeCanvas Technologies website (https://sites.google.com/lifecanvastech.com/protocol/).[21,86] The following steps detail the workflow: Samples were cleared for 7 days with Clear+ delipidation buffer, followed by batch labeling in SmartBatch+ with 5 μg anti-Rabbit pS6 (Invitrogen Cat# 44-923G), 17 μg anti-Mouse NeuN antibody (Encor MCA-1B7) per brain. Fluorescently conjugated secondary antibodies were applied in 1:2 primary/secondary molar ratios (Jackson ImmunoResearch). Labeled samples were incubated in EasyIndex (LifeCanvas Technologies) for refractive index matching (n = 1.52) and imaged using SmartSPIM (LifeCanvas Technologies) with a 4 μm z-step, 1.8 μm xy pixel size, and wavelengths of 488 nm for NeuN detection and 561 nm for pS6 detection. Image analysis was conducted following the procedures as previously published.[21,86] Atlas Registration: Samples were registered to the Allen Brain Atlas (Allen Institute: https://portal.brain-map.org/) using an automated process (alignment performed by LifeCanvas Technologies). A NeuN channel for each brain was registered to an average NeuN atlas (generated by LifeCanvas Technologies using previously-registered samples). Registration was performed using successive rigid, affine, and b-spline warping algorithms (SimpleElastix: https://simpleelastix.github.io/). Cell Detection: Automated cell detection was performed by LifeCanvas T echnologies using a custom convolutional neural network created with the Tensorflow python package (Google). The cell detection was performed by two networks in sequence. First, a fully-convolutional detection network (https://arxiv.org/abs/1605.06211v1) based on a U-Net architecture (https://arxiv.org/abs/1505.04597v1) was used to find possible positive locations. Second, a convolutional network using a ResNet architecture (https://arxiv.org/abs/1512.03385v1) was used to classify each location as positive or negative. Using the previously-calculated Atlas Registration, each cell location was projected onto the Allen Brain Atlas in order to count the number of cells for each atlas-defined region.

Single-nucleus RNA sequencing

Animals received 3-day treatment of rapamycin and/or leptin were anesthetized under 5% isoflurane 4-hour post last injection. ARC was microdissected under a stereo microscope in pre-chilled dissection buffer and immediately transferred to dry ice prior to downstream nuclei extraction at the same day. After dissection, frozen tissues on dry ice were immediately transferred to Teflon homogenizer containing 1 ml pre-chilled 0.1% NP40 (IGEPAL CA-630) lysis buffer (Sigma-Aldrich, Cat# I8896) and homogenized for 15-30 times using a pellet pestle on ice. Homogenized samples were incubated for another 10-15 min on ice, followed by passing through a 70 μm Flowmi Cell Strainer and a 40 μm Flowmi Cell Strainer (Millipore Sigma). The collected flowthrough was centrifuged at 500–1000 rcf for 5 minutes at 4°C, and the pellets were completely resuspended in 1 ml of staining buffer. Subsequently, 1 ml of 20% iodixanol was carefully loaded beneath the staining buffer at 4°C. Samples were centrifuged at 10000 rcf for 20 min at 4°C. Supernatant containing debris was carefully removed. Pellets were resuspended in staining buffer containing anti-NeuN Alexa 647 antibody (abcam, Cat# ab190565) and HashTag antibodies (1 μl for labeling ∼1 x 10^6 nuclei, BioLegend, TotalSeqB anti-Nuclear Pore) in order to enrich neurons and multiplex samples. After antibody incubation and rotating for 30 min at 4°C, samples were washed with staining buffer without antibodies for 3 times. Samples were resuspended in FACS buffer after last-round wash and sent for FACS sorting. Hoechst 33342 (ThermoFisher Scientific, Cat# H3570) were added at a final concentration of 0.2 mM to label nuclei. Sorted nuclei were sent for downstream 10X genomics 3' RNA-seq with feature barcode library preparation and sequenced using NovaSeq sequencer or DNBseq sequencer at BGI with ∼30000 reads/nuclei on average. Dissection buffer contains 1X HBSS, 2.5 mM HEPES-KOH [pH 7.4], 35 mM Glucose, 4 mM $NaHCO_3$, and Actinomycin D (Sigma-Aldrich, Cat# A1410) at a final concentration of 20 μg/ml. NP40 lysis buffer contains 10 mM Tris-HCl [pH 7.4], 10 mM NaCl, 3 mM $MgCl_2$, 0.1% NP40 dissolved in nuclease-free water. For 1 ml NP40 lysis buffer, 1 μl DTT, 25 μl 20 U/μl SUPERaseIn (ThermoFisher Scientific Cat# AM2696), 12.5 μl 40 U/ μl RNasin (Promega Cat# N2615), 10 μl protease and phosphatase inhibitor cocktail (100X; ThermoFisher Scientific Cat# 78442), 40 μl 1 mg/ml Actinomycin D were added right before use. 20% iodixanol buffer contains 0.25M sucrose, 25mM KCl, 5mM $MgCl_2$, 20mM Tricine-HCl [pH 8.0] and 20% Iodixanol dissolved in nuclease-free water. DTT, Superasine, Rnasin and protease inhibitors were added at the same concentration as NP40 lysis buffer right before use. Staining buffer contains 2% BSA, 0.05% NP40 dissolved in nuclease-free 1X PBS. Superasine, Rnasin and protease inhibitors were added at the same concentration as NP40 lysis buffer right before use. FACS buffer contains 2% BSA dissolved in nuclease-free 1X PBS buffer. Superasine, Rnasin and protease inhibitors were added at the same concentration as NP40 lysis buffer right before use.

snRNA-seq analysis

The fastq files were aligned to mouse genome (mm10), and the expression levels in each cell were estimated with Cellranger (v 6.0.0). The gene expression count matrix for each sample was processed with the following steps: (1) Estimate doublet with Scrublet (https://github.com/swolock/scrublet)[88]; (2) Estimate and correct the ambient RNA contaminations with SoupX (https://github.com/constantAmateur/SoupX)[89]; (3) Load the corrected counting matrix into Seurat object with log normalization; (4) Calculate the proportion of UMIs from mitochondrial genes; (5) Demultiplex with hashtag oligos followed the Seurat vignette (https://satijalab.org/seurat/articles/hashing_vignette.html); (6) The cells assigned as doublets or mitochondrial content greater than 1% were removed. The Seurat objects were integrated by following the RPCA workflow (https://satijalab.org/seurat/articles/integration_rpca.html).[90] The number of PCs used for UMAP calculation was selected with elbow plot.[91] Then, the clustering was calculated with Leiden algorithm.[92] To select the optimized resolution, the resolution was tested from 0.1 to 1.0 and was selected with clustree. The Chow_HFD was assigned as the reference dataset. The clustering information were mapped and transferred from the reference to OB_RAP_VEH datasets by following the Seurat vignette (https://satijalab.org/seurat/articles/integration_mapping.html). The differential gene expression of each comparison was performed with Seurat::FindMarkers() with logfc.threshold greater than 0.14, and raw p values were corrected using p.adjust() with the 'BH' method. Significant differential expression genes were defined as $\log_2$ (Fold Change) greater than 0.26 or less than -0.26, and corrected p values less than 0.05.

Histology

Mice were transcardially perfused with PBS (Fisher Scientific, Cat# BP39920) followed by 4% paraformaldehyde (PFA, EMS Cat# 15714-S). Brains were dissected and post-fixed in 4% PFA at 4°C overnight. Brains were sectioned into 50-μm coronal slices using a vibratome (Leica VT1000 S). For immunohistochemistry, brain sections were blocked in the blocking buffer for an hour at room temperature. Blocking buffer contains 0.1% Triton X-100 (ThermoFisher Scientific Cat# 85111) in PBS, 3% bovine serum albumin (Sigma Cat# A9647-500G), 2% normal donkey serum (Jackson ImmunoResearch Cat# 017-000-121). For pSTAT3 staining, sections were first rinsed in 1% H2O2 + 1% NaOH in H2O for 20 min, at room temperature, then transferred to 0.3% glycine in 1X PBS for 10 min, at room temperature prior to blocking. Sections post blocking were then incubated with primary antibody (rabbit anti-Phospho-S6, Invitrogen, Cat# 44-923G, 1:1000 dilution; rabbit anti Phosphp-STAT3, Cell Signaling, Cat# 9145 1:500 dilution; chicken anti GFP, 1:1000 dilution, abcam, Cat# ab13970) for 2 days at 4°C. Sections were then washed and incubated with secondary antibody (donkey anti-chicken IgG Alexa 488, Jackson Immunoresearch, Cat# 703-546-155, 1:1000 dilution; donkey anti-rabbit IgG Alexa 594, Invitrogen, Cat# A21207, 1:500 or 1:1000 dilution) for 1 hour at room temperature, washed again, mounted with DAPI Fluoromount-G (Southern Biotech Cat# 0100-20) and imaged with SlideView microscope (VS200, Olympus). Images underwent minimal processing (such as adjusting brightness and contrast linearly) performed using ImageJ. The CellCounter plugin for ImageJ was used to quantify numbers and percentages of co-localizations from sections.

Brain sections in Figure S15E were rinsed in 0.02 M KPBS (pH 7.4), followed by pretreatment in a water solution containing 1% hydrogen peroxide and 1% sodium hydroxide for 20 min. After extensive washes in 0.02 M KPBS, the sections were incubated in 0.3% glycine for 10 min and then 0.03% lauryl sulfate for 10 min. Thereafter, the sections were blocked in 3% normal donkey serum for 1 h, followed by incubation in rabbit anti-pSTAT3^{Tyr705} (1:1000, Cell Signaling, #9145) or rabbit anti-pS6 (Invitrogen Cat# 44-923G) for 48 h or 24h, respectively. For the immunofluorescence reactions, sections were rinsed in KPBS and incubated for 120 min in Fab fragment donkey anti-rabbit AlexaFluor^{488} (1:500, Jackson Immuno Research, Cat# 711-547-003).[93] Thereafter, sections were washed three times in 5% formalin for 10 min and then washed three times in 0.02 M KPBS for 5 min. Sections were then incubated with AgRP antibody (1:1000 Phoenix Pharmaceuticals, Cat# H-003-57) overnight at room temperature. After washing in 0.1 M PBS, the sections were incubated for 30 min with the secondary antibody AlexaFluor^{594} (1:500, Jackson Immuno Research, Cat# 711-585-152) diluted in 0.02 M KPBS. After three washes in 0.02 M KPBS for 10 min, the sections were mounted onto gelatin-coated slides and coverslipped with DAPI Fluoromount-G (Southern Biotech Cat# 0100-20). The percentage of pSTAT3-positive AgRP neurons was determined upon the subcellular detection of AgRP using a modified protocol.[94,95] Briefly, DAPI-positive cells in the arcuate nucleus of the hypothalamus were segmented on QuPath and the subcellular AgRP staining was counted in single-cell ROI showing pS6 or pSTAT3 signal.

Slice preparation and electrophysiology

Acute coronal hypothalamic brain slices (200 μm) were prepared from POMC-eGFP (8-44 weeks old). Mice fed either on chow diet, or high fat diet for a minimum of 16 weeks. Chow data were generated from 8-12 week old mice (n=7, 3-8 neurons per mouse). DIO data were generated from 20-44 week old mice (n=33, 1-10 neurons per mouse). Vehicle-treated DIO data were generated from 33 week old mice (n=4, 6-12 neurons per mouse) and rapamycin-treated DIO data were generated from 32-33 week old, (n=4, 5-10 neurons per mouse). Mice were anesthetized with isoflurane prior to decapitation and removal of the entire brain which was immediately submerged in ice-cold 'slicing' solution containing (in mM): 85 NaCl, 2.5 KCl, 0.5 CaCl2, 4 MgCl2, 25 NaHCO3, 1.25 NaH2PO4, 64 sucrose, 25 glucose. This solution was bubbled with 95% O2 and 5% CO2, pH 7.4. Coronal hypothalamic slices (200μm) were made with a moving blade microtome (VT1000S, Leica). The slices were kept at 32 °C for 40 min in recording solution containing (in mM) 125 NaCl, 2.5 KCl, 1.25 NaH2PO4, 26 NaHCO3, 10 glucose, 2 CaCl2 and 1 MgCl2, pH 7.4 when bubbled with 95% O2 and 5% CO2 before being kept at room temperature prior to recording. Cell-attached patch-clamp recordings were made in voltage clamp configuration with 0pA holding current at room temperature from eGFP-expressing neurons in the arcuate nucleus. Neurons were visualized using epifluorescence and patched under DIC imaging on an upright microscope (Zeiss Axioskop 2FS Plus) equipped with a CCD

camera (Hamamatsu). Patch pipettes pulled (Narishige PP-830) from borosilicate glass (Sutter Instrument) had tip resistances of 7–11 MΩ and were filled with K-gluconate internal containing (in mM): 135 potassium gluconate, 4 KCl, 0.05 EGTA, 10 Hepes, 4 MgATP, 10 Na-Phosphocreatine, pH adjusted to 7.3 with KOH, 290 OSM. All chemicals were obtained from Sigma. Leptin stock was prepared in PBS (1mg/ml or 100μM), then diluted in ASCF (100nM) and bath applied for 20 minutes via perfusion. Recordings were acquired with an Axopatch 200B amplifier, filtered to 2 kHz and digitized at 10 kHz (pClamp10 software, Molecular Devices). Data were analyzed using IGOR Pro (Wavemetrics) and NeuroMatic (http://www.neuromatic.thinkrandom.com/). Mean firing rate was detected in 10 second bins and maximum firing rate was recorded in each condition. Baseline firing rate was calculated in the first minute of recording, ASCF was calculated in the minute before peptide application. Neurons were considered excited or inhibited by leptin if firing changed more than 10%. For i.p. injections DIO mice fed on high fat diet for more than 16 weeks were injected either with rapamycin (2 mg/kg) or vehicle once a day for 3 consecutive days before brain slice preparation.

Viral injections into the ARC

Cre-inducible AAV5-hSyn-DIO-mCherry (Addgene Cat# 50459-AAV5) and AAV5-mCherry-flex-dtA (plasmid was obtained from Addgene Cat# 58536, AAV viruses were packaged at Janelia Research Campus) viruses were injected into ARC of POMC-Cre+ animals using stereotactic surgery as follows: Mice were anesthetized with 3% isoflurane in oxygen, placed in a stereotaxic apparatus (Kopf Instruments) and kept at 1.5% isoflurane (Henry Schein Cat# 11695-6776-2) during surgery. Viruses were bilaterally delivered using a borosilicate glass pipette connected to Nanoject (Drummond, Cat# 3-000-203-G/X) in ARC (200 nl per coordinate, 50 nl/min). The coordinates to locate ARC were relative to the bregma: AP/DV/ML = −1.75/−5.95/±0.25 mm, AP/DV/ML = −1.75/−5.75/±0.25 mm. After finishing injection at each coordinate, syringes were held at the coordinate for another 3 minutes. Animals were allowed to recover (and adjust eating habits) for 8 weeks post-surgery, before being used in experiments. Plasmids containing guide-RNAs were designed, customized and generated at VectorBuilder. Wdr24-gRNAs, gRNA1 (5'-3'): GGGGTCATGCGGATGACGCC, gRNA2 (5'-3'): CATCTTCTTCAAGCGCAAGT; Rheb-gRNAs, gRNA1 (5'-3'): ACCAAGTTGATCACGGTAAA, gRNA2 (5'-3'): GTTCTCTATGGTTGGATCGT. Plasmids were then packaged into AAV viruses at Janelia Research Campus.

Metabolic cages

Diet-induced obese mice were singly housed in a climate-controlled (temperature: 22 °C; humidity: 55%; 12-hour light–12-hour dark cycle) automated home cage phenotyping system (TSE) with *ad libitum* access to water and high-fat-diet. After 7 days of adaptation to the TSE cage, receiving daily mock IP injections, the mice were treated daily with IP vehicle or IP 2 mg/kg Rapamycin for 6 days (Figures S7E–S7H). Data were collected and analyzed as recommended by the manufacturers. Energy expenditure and respiratory exchange ratio (RER) were measured by an indirect gas calorimetry module recording open circuit oxygen consumption and carbon dioxide production (VO_2 and VCO_2). Locomotor activity was recorded as beam breaks converted into distance/velocity, measuring activity in three dimensions and analyzed in the metabolic cage using custom software. Statistical assessment of the data was conducted using CalR software (https://www.calrapp.org).

QUANTIFICATION AND STATISTICAL ANALYSIS

Statistics and reproducibility

We conducted statistical analyses using GraphPad Prism 9.0. Throughout the paper, values were reported as mean ± SEM (error bar). Each statistical test performed was denoted in the figure legends. P-values for pair-wise comparisons were obtained using two-tailed student's t-test. P-values for two independent group comparisons were either obtained using two-tailed student's t-test or nonparametric Mann-Whitney test based on data distributions. P-values for multiple group comparisons were conducted using one-way or two-way ANOVA (with repeated measures when possible) based on the number of factors and corrected for multiple comparisons using Fisher's LSD test, Tukey's test or Sidak's test, indicated in the figure legends. The experiments were not randomized. Data for each experiment were repeated with at least two different cohorts. Representative trial data or pooled data from multiple cohorts were used for conducting statistics and plotting figures. The investigators were not blinded to allocation during experiments and outcome assessments.